Peripheral CGRP engages brain-wide electrical network activity of migraine

Micah Johnson[1,2], Maureen Eberle[1,2], Ian Hultman[3], Xinyu Zhang[3], Yassine Filali[1,2,] Benjamin Hing[1], Alli Jimenez[1], Molly Matkovich[1], Sara Mitchell [1,2], Anjayooluwa Adegboyo[5], Radha Velamuri[1], Julia Miller[1], Kung-Sik Chan[3], Sanvesh Srivastava[3], Rainbo Hultman[1,4]

1 Department of Molecular Physiology and Biophysics, University of Iowa, Iowa City, IA, USA

2 Interdisciplinary Graduate Program in Neuroscience, University of Iowa, Iowa City, IA, USA

3 Department of Statistics and Actuarial Science, University of Iowa, Iowa City, IA, USA

4 Department of Psychiatry, University of Iowa, Iowa City, IA, USA

5 University of Maryland Baltimore County, Baltimore, MD, USA

Correspond with Dr Hultman (Dept. of Molecular Physiology & Biophysics, Iowa Neuroscience Institute, 51 Newton Rd., 6-510 Bowen Science Building, Iowa City, IA, 52242, USA; 319-335-2855 (o), 919-451-6906 (c); rainbo-hultman@uiowa.edu.

Keywords: migraine, CGRP (calcitonin-gene related peptide), brain networks, early life stress

Summary

Migraine is a disorder consisting of severe, recurrent headaches and debilitating sensory symptoms which often include affective symptoms or comorbidities such as depression, anxiety, and irritability. As such, migraine is a complex nervous system disorder that involves integration of many modalities across the brain. This makes migraine a complex systems neuroscience problem represented by the confluence of sensory, pain, cognitive, autonomic, and affect-related circuits. Thus, it is essential to understand how neuronal activity across various brain regions implicated in migraine is coordinated during migraine pathophysiology. Using a calcitonin gene-related peptide (CGRP) mouse model of migraine, we probed neural oscillatory activity in the anterior cingulate cortex, amygdala (BLA and CeA), thalamus (Po, VPM, and MDthal), and parabrachial nucleus following peripheral administration of CGRP. We identified three frequency bands in which directional signals occur in this network and found that power in these frequencies across the network was lower than vehicle within 10 minutes of peripheral CGRP exposure, which was sustained for (~40-50 min). Coherence, on the other hand, was mostly disrupted in CeA brain region pairings, and took on a shorter timecourse. Sumatriptan partially blunted or reversed these CGRP-induced network responses, especially with regard to amygdala power and coherence pairings. Early life stress, which has been shown to increase the likelihood of migraine in adulthood in humans, exacerbated CGRP-induced migraine-related behavioral phenotypes and induced corresponding network changes in LFP power in the CeA and Po and coherence in Po-related pairings. Clustering based on a changepoint analysis of coherence identified individual mice hypersusceptible to migraine. Overall, our findings demonstrate coordinated brain-wide network activity by which migraine is mediated in the brain in response to peripheral CGRP.

Intro

Migraine is an intricate and incapacitating neurological disorder and the second leading cause of global disability [1]. Migraine is characterized by recurrent headache episodes spanning 4 to 72 hours with various sensory anomalies including hypersensitivities such as, photophobia, phonophobia, osmophobia, and allodynia [2]. However, it is important to recognize that migraine is far more involved than just headache, and frequently occurs over characteristic stages including prodrome, aura (impacts ~20% of individuals with migraine), headache, postdrome, and interictal phases [3]. In addition to sensory hypersensitivities, many of these phases of migraine can include changes in perception, cognition, autonomic nervous system regulation, and mood. While the underlying origin of migraine has been historically debated in terms of central and peripheral mechanisms, there is growing consensus of both peripheral and central contributors to migraine [4]. Regardless of origin, it is clear that migraine engages multiple functional domains (cognition, perception, emotion/affect etc.) that are known to have causal origins in the brain.

Clues to brain mechanisms engaged in migraine stem from a combination of symptomology and imaging studies. Imaging studies have revealed altered functional connectivity within and between brain networks in migraine patients and structural differences in pain-related regions. These changes have been observed not only during migraine attacks but also in the interictal period [3,5-7]. A number of studies have indicated that a large part of what makes migraine so severe and debilitating comes from the aversive aspect of pain, which is greater for pain in the head compared to pain in periphery [8,9]. Head pain is ranked as more emotionally salient and severe than other types of peripheral pains. For example, a study in humans demonstrated that repeated application of noxious heat to the face induces sensitization whereas the same application of noxious heat to the hand induces habituation [8]. Additionally, despite having similar pain intensity levels, fear induced by pain was quantitatively regarded as more severe in the face than in the extremities [10].Thus, we focused our initial efforts toward

understanding endogenous neural activity across several brain regions with an emphasis on regions involved in the emotional salience of head pain and mood aspect of migraine: anterior cingulate cortex (ACC), central amygdala (CeA), basolateral amygdala (BLA), posterior thalamus (Po), ventroposteromedial thalamus (VPM), medialdorsal thalamus (MDthal), and parabrachial nucleus (PBN), all of which have been implicated in the pathophysiology of migraine [3,11]. The ACC is a key region in pain processing and more specifically, emotional processing of pain [12]. Reduction in ACC grey matter is correlated with frequency of migraine attacks in migraine patients [13]. The amygdala is implicated in affective pain processing and the perception of such pain [14,15]. Resting functional connectivity patterns in a network involving the amygdala have been shown to discern migraine and healthy control patients [16]. Further, increased connectivity patterns between the nucleus accumbens and the amygdala were found during the preictal phase compared to the ictal phase demonstrating the involvement of the amygdala in specific phases of migraine[17]. The thalamus is broadly implicated in the integration of sensory information and has been associated with migraine-related allodynia, photophobia , and hypersensitivity to negative emotional stimuli [18-21]. Additionally, altered thalamo-cortical functional connectivity patterns have been reported in migraine [22]. Optogenetic stimulation of the posterior thalamus was found to induce photophobia-like behavior in the absence of anxiety [23]. Finally, the PBN is a critical sensory relay center and is important for homeostatic function, arousal, cravings, thirst, nociception and regulation of affective responses [24,25]. Altered connectivity patterns across subcortical-cortical networks that include the PBN have been found in migraine patients during the preictal phase [5,11,26,27]. Importantly, the PBN contains CGRP projections to the central amygdala, which has been demonstrated to play an important role in the emotional aspect of pain [14,24,28] as well as projections to the thalamus, which convey nociceptive information to higher order cortical regions [29] . Overall, human imaging studies point to brain-wide connectivity changes in migraine, however, ultimately endogenous

multi-region brain network studies in disease models are required to understand the ways in which brain regions communicate on a timescale of neuronal activity.

The ways in which endogenous brain-network activity is engaged and coordinated in mouse models of migraine remain largely unknown. Preclinical models of migraine allow for probing of neuronal circuitry across time in a way that can help better understand the actual mechanisms underlying the interconnected circuitry that leads to migraine. Developing an understanding of systems-level brain activity in preclinical models of migraine holds great promise for a new era of migraine research and therapeutic development [30].

One of the best characterized and most robust animal models of migraine makes use of calcitonin gene-related peptide (CGRP) to induce a migraine-like phenotype in mice. This model demonstrates validity to the human disorder in three important ways: face validity (the model displays a similar disease phenotype as in humans) [31] construct validity (the model shares the same underlying cause of the disease in humans) [32,33], and predictive validity (treatments that are effective in humans are effective in the model) [32,34]. CGRP has emerged as a neuropeptide of prominent importance in migraine pathophysiology. Key evidence for the involvement of CGRP in migraine is that CGRP levels are elevated during migraine attacks [35-37]. Blocking CGRP signaling can also alleviate migraine symptoms in both humans and rodent models [38]. Additionally, injection of CGRP (either central or peripheral) leads to a delayed migraine-like headache in humans [33] and preclinical migraine-like phenotypes (e.g., light aversion, spontaneous pain, and allodynia) in rodents [31]. There has been mounting evidence that CGRP acts on receptors peripherally, with indirect impacts that reach the brain [4,30]. CGRP has also been shown in preclinical models to evoke a migraine-like response when injected directly into the brain [23]. However, the nature of impact of peripheral CGRP on the brain remains one of the fundamental questions in solving the mystery of migraine. Elucidating the impact of peripheral CGRP on brain network activity is

an important hurdle to overcome in order to understand how different functional systems demonstrate interconnected activity, such as sensory hypersensitivities in migraine.

In this manuscript, we aim to investigate the brain network dynamics underlying migraine at both high spatial and temporal resolution using a CGRP mouse model of migraine. We employ multi-site *in vivo* neurophysiological recordings in freely behaving animals to monitor changes in brain activity and connectivity in response to peripheral CGRP administration over time. We then further probe brain network activity with anti-migraine medication, sumatriptan, and an environmental stressor known to increase the likelihood of migraine in humans. Finally, we applied a changepoint analysis in order to identify network-wide changes associated with migraine-like phenotypes.

Results

Peripheral injection of CGRP induces light-aversive behavior in electrode-implanted animals

To gain insight into brain mechanisms of migraine, we implanted and recorded neurophysiological activity from multi-site electrode wires in the anterior cingulate cortex (ACC), basolateral amygdala (BLA), central amygdala (CeA), mediodorsal thalamus (MDthal), posterior thalamus (Po), ventroposteromedial thalamus (VPM), and bilateral parabrachial nucleus (LPBN/RPBN) (Figure 1A, Supplementary Figure S1). Such an approach allows us to quantify spatiotemporal dynamics following peripheral CGRP administration based on local field potential (LFP) activity and subsequently perform behavioral studies to phenotypically validate the effect of peripheral CGRP (Figure 1B).

We first wanted to determine whether our implanted animals exhibit similar light aversive behavior following CGRP administration. The light/dark assay has been utilized to assess migraine-like behavior during the CGRP mouse model of migraine [31]. Light aversion was assessed using the average amount of total time spent in light (in seconds) during the first 15 minutes of a 30-minute testing period (Figure

1C). We used a repeated measures design to compare unimplanted and implanted animals in response to CGRP and performed a control that determined that there is no effect of repeated injection over days using groups that received PBS injections both days and/or CGRP on the treatment day). We used a three-factor mixed-effects model to evaluate the impact of implant, CGRP, and repeated measures. There was no significant interaction between CGRP treatment and the electrode-implanted condition ($p = 0.79$, Figure 1D). However, CGRP treatment did result in decreased time spent in the light on the CGRP treatment day compared to the vehicle day ($p = 0.01$, Figure 1E). We found no significant effect of repeated injection ($p = 0.67$, Figure 1E), nor due to the day itself ($p = 0.77$). Overall, we demonstrated that our electrode-implanted animals exhibit the same phenotype as unimplanted animals, consistent with phenotypes previously published [32]. We also analyzed the total amount of time spent in light and resting time in dark across all implanted animals utilized in subsequent experiments (Figure S2). Again, implanted animals injected with CGRP exhibited decreased time spent in light during all 30 minutes ($n = 31$, $p <0.001$, Figure S2) and the first 15 minutes of the light/dark test ($n = 31$, $p<0.001$ (Figure S2).

LFP directionality across the bilateral parabrachial, central amygdala, and thalamic (MD/Po/VPM) subnetwork

To identify LFP oscillation frequencies of interest, we calculated directionality of information flow from one brain region to another between brain region pairs based on a temporal lag approach in which phase offsets are introduced. Multiple studies have demonstrated important biology and behavioral predictions in frequencies where one region of a circuit clearly leads another between coherent brain regions [39-45]. The temporal offset at maximal synchrony indicates which region is leading and lagging at each frequency [40,43,46-48]. In order to specify precise frequency bands in which information flow appears to be directional from one region to another, we applied a fused lasso approach, enforcing a lasso

penalty on absolute value differences between contiguous frequencies in phase offset (see methods, Figure 2).

Given the roles of the CeA and thalamic nuclei in affect and migraine, we hypothesized that the PBN-CeA-Thalamus regions might represent a significant subnetwork and we focused on the directional relationships between these regions. We utilized the lasso regression on the greatest mean temporal phase offsets within these pairings to determine our frequency bands of interest (Figure 2). We found that CeA leads all of the thalamic (MD/Po/VPM) and bilateral parabrachial (LPBN/RPBN) nuclei in the 4-7 Hz frequency range (Figure 2). Continuing in this subnetwork, we found that all other regions led the CeA in the 8-13 Hz range (Figure 2).

CGRP induces decreases in LFP power across migraine-related brain regions

Our analysis indicates that 4-7 Hz is a frequency band in which the CeA is a major leading region. This frequency range, often referred to as *theta,* has been identified in various brain regions to be involved in functions like sleep, memory, and anxiety [47,49-54] . We hypothesized that we would observe significant differences in LFP power across each of the brain regions we implanted in the 4-7 Hz frequency. All data were normalized to the baseline period before plotting, and the time series was evaluated starting from the 30-minute mark, corresponding to the injection time for each animal. Because we're interested in both the magnitude of response as well as the time-dependence, we employed a Function on Scalar General Additive Model analysis (FOS) followed by an FDR correction, testing the hypothesis that there are differences in LFP power across time in response to peripheral CGRP within each brain region. This analysis revealed that LFP power in the 4-7 Hz frequency band was significantly different across all regions we implanted over time when animals were treated with CGRP compared to when treated with PBS (Figure 3). Across all eight brain regions (ACC, BLA , CeA, MDthal, Po VPM, LPBN, and RPBN) there was a decrease in LFP mean logpower following CGRP administration compared to vehicle control

initially following the injection point (Figure 3A) and gradually increasing until reaching a similar mean logpower under the vehicle condition (p= 3.77e-16, Figure 3B-H). ACC (Figure 3B) and CeA (Figure 3C) contained the greatest relative changes immediately post-injection. The peak changes in power occurred around 10-30 minutes post-injection, with the effects primarily resolving by 45 minutes post-injection, and completely resolving by 60-75 minutes post-injection. These data are highly consistent with what has been reported in terms of behavioral response to peripheral CGRP using facial grimace[55].

We also hypothesized that the 8-13 Hz frequency band was a relevant frequency band as all of the other brain regions led the CeA in the 8-13 Hz frequency band (Figure 2). Similar to the 4-7 Hz frequency band, we observed changes in mean logpower in all regions of our network, though minimal in the 1-3Hz band (Supplemental Figures S3-4). Again, the ACC (Supplemental Figure S4) contained the greatest relative difference, followed by the CeA and LPBN and overall power changes resolved by around 45-60 minutes post-injection (Supplemental Figure S4). Overall, we observed changes in LFP power across all brain regions of the network in two different frequency bands in response to peripheral CGRP, supporting centrally-mediated activity during a peripherally-induced migraine brain state.

CGRP induces disruptions in LFP coherence across migraine-related brain regions

Next, we wanted to evaluate how connectivity across the network was altered, if at all, during a CGRP-induced migraine brain state, especially between CeA-brain region pairings. To answer the question of how brain regions communicate with each other across time during a migraine-like brain state, we analyzed coherence among brain region pairings following CGRP administration compared to vehicle conditions. We focused on CeA and Po-related pairings, given the central role of these brain regions in migraine.

High mean coherence was observed across the major pairings of our network (e.g. pairings with CeA and Po) within the 1-13 Hz frequency range +/- CGRP (Figure 4A). Given our directionality analyses, we

focused on evaluating coherence changes in the 4-7 Hz and 8-13 Hz bands. Similar to CGRP-induced changes in power, the disruptions in coherence in response to CGRP were most pronounced in the first 10 minutes post-injection, but unlike the power, they largely resolved much faster, within ~20 minutes post-injection (Figure 4B). The FOS model demonstrated that there are significant disruptions in coherence across brain region pairings in response to CGRP compared to vehicle (Figure 4C). All LFP data was normalized to baseline periods and plotted starting at the 30-minute point onward providing a stabilizing transform while preserving direction, as log odds coherence. In both the 4-7 Hz band and 8-13 Hz frequency band, we observed the greatest CGRP-disrupted coherence between the CeA-LPBN, CeA-Po, and BLA-VPM (p= 3.77e-16, Figure 4D-F, Supplemental Figure S5-6). The relative difference in mean log-odds coherence of 0.23 between the CeA and LPBN in the 4-7 Hz band (Figure 4D) and 0.24 between the BLA and VPM in the 8-13 Hz band (Figure 4F) were the greatest amongst all pairings immediately following the injection. The maximal difference between the CeA and Po was 0.20 at 7 minutes post-injection (Figure 4E). We observed the largest power differences and the most significant pairings in the BLA, CeA, and ACC in response to CGRP, so it was also important to evaluate coherence in the context of these findings. Additionally, given our overall network connectivity hypotheses, we were interested in whether CGRP disrupted coherence between the amygdala, thalamus, and ACC as these regions form key circuits involved in chronic pain [56] and pain perception [57]. Notably, BLA-VPM coherence exhibited the most temporally sustained disruptions across time (~35 minutes post-injection, p= 3.77e-16, Figure 4G). Among ACC-pairings, coherence between ACC-BLA (p= 0.02, Figure 4H) and ACC-CeA (p= 1.21e-7, Figure 4I) increased following CGRP, particularly just prior to 40 minutes post-injection which was much later than the other brain region pairings. These findings support the critical role of electrical activity alterations in the amygdala during migraine attacks. Disruption of BLA/CeA-related LFP patterns appear to underlie the endogenous migraine brain state, leading to the painful and affective symptoms associated with migraine.

Coadministration of CGRP and Sumatriptan partially reverses the effect of CGRP

We next investigated how CGRP-induced migraine-related brain network dynamics respond to a drug commonly used for acute migraine treatment, sumatriptan[58]. Sumatriptan, a common migraine abortive, is a serotonin 1B, D, and F agonist that was originally thought to have peripheral mechanisms of action but recently has been found to act in the brain as well[59,60]. Brain network dynamics measured by fMRI of thalamus and amygdala have been demonstrated to be altered in response to sumatriptan [61]. We hypothesized that coadministration of sumatriptan and CGRP would attenuate some or all of the changes in power and coherence induced by CGRP. However, it is worth noting that sumatriptan has had somewhat limited efficacy in rodent models [32,55].

To assess whether sumatriptan effectively blunted the CGRP response, we compared responses between CGRP alone and sumatriptan+CGRP (Figure 5A). We first considered the direction of the sumatriptan+CGRP relative to CGRP and vehicle. Interestingly, the ACC, BLA, and CeA were the only regions in which co-administration of sumatriptan+CGRP attentuated the CGRP response, particularly in the 8-13 Hz frequency band (Figure 5B). The greatest relative differences in mean log-power between the sumatriptan+CGRP and CGRP-only conditions was observed in the 8-13 Hz frequency band in the BLA and CeA, with the coadministration reversing the effect of CGRP alone ($p= 3.77e-16$, Figure 5C-D). Similar effects were seen in the ACC ($p= 3.77e-16$, Figure 5E).

We then assessed the effect of sumatriptan+CGRP on coherence (Figure 5F). We particularly evaluated the sumatriptan coherence response in the 30-50 minute time range (0-20 minutes post-injection) in which it was most disrupted by CGRP. Beginning with the three region pairings where CGRP was found to most disrupt coherence, we observed significant differences in coherence between the CeA-LPBN ($p= 7.26e-10$, Figure 5G) after sumatriptan+CGRP, but no difference in CeA-Po ($p= 0.92$, Figure 5H). The coherence changes between the LPBN and Po, while significant, were not in the direction of CGRP

reversal (p= 3.77e-16, Supplement Figure S7). Interestingly, the brain region with the greatest number of pairings reaching statistical significance and the greatest effect of sumatriptan blunting CGRP response was BLA, including BLA-VPM (p= 3.77e-16, Figure 5I) and ACC-BLA (p= 3.77e-16, Figure 5J). Diminution of the impact of CGRP on coherence were also observed between the ACC and CeA (p= 5.31e-9, Figure 5K). Several other region pairings involving the parabrachial and thalamic nuclei showed significant changes in the same direction as CGRP rather than a reversal (Supplemental Figure S7), suggesting that sumatriptan induces distinct connectivity patterns within these pathways.

In summary, coadministration of sumatriptan and CGRP blunted the impact of CGRP on LFP power in the ACC, BLA, and CeA, especially at later time points where the impact of CGRP is beginning to wane. Further, sumatriptan blunted CGRP-induced disruptions in coherence, especially in BLA-related region pairings. These findings suggest that while sumatriptan effectively mitigates CGRP-induced disruptions in LFP power in some key limbic regions, it doesn't ablate all CGRP-induced effects and even introduces new connectivity patterns, making its overall impact on migraine brain network connectivity complex.

ELS exacerbates migraine-related phenotypes in CD1 mice

Stress, especially stress experienced early in life, is a naturally-occurring event in the life of both humans and rodents that has been demonstrated to play an important role in migraine and has been implicated as altering plasticity in several affect-related brain regions including the ACC, BLA/CeA, and PBN [62-65]. Specifically, adverse childhood events, also referred to as early life stress (ELS), is associated with migraine diagnosis in adulthood [66,67]. As such, we reasoned that we could understand more about how migraine network activity is regulated by studying the impact on behavior and network activity of this natural, ethologically and biologically relevant perturbant. We induced ELS in CD1 mice by utilizing a

maternal separation stress paradigm with early weaning and limited nesting to test the effect of another manipulation on our neurophysiological recordings (Figure 6A).

While previous studies have found that ELS enhances migraine-like phenotypes in rats [68] and female C57Bl/6J mice [69], this relationship hasn't previously been identified in the context of CGRP. A total of 52 litters were utilized for experiments, and animals were split into balanced groups according to weight and cohort prior to experiments (Figure 6A). Animals were randomly divided in an age-balanced way such that half of the litters underwent ELS and half remained group-housed (control). To assess the effect of ELS on migraine-related phenotypes, we administered peripheral PBS or CGRP to both groups (Control-Veh/Control-CGRP and ELS-Veh/ELS-CGRP). Following our stress paradigm (see Methods), we waited until mice reached adulthood (P66-69) performed behavioral assays to assess anxiety-like and migraine-like behavior. We hypothesized that ELS would exacerbate migraine-related phenotypes in mice treated with CGRP compared to control mice.

First, we assessed anxiety-like behavior at P66-69 using the elevated plus maze to ensure that animals exhibited an anxiety-like phenotype during adulthood. We found that male and female mice that underwent ELS spent less time in the open arms of the elevated plus maze ($p = 0.04$, $t(91) = 2.11$, unpaired t test) which indicates that the ELS sufficiently stressed the animals into adulthood (Figure 6B).

Cutaneous allodynia is present in 60% of patients with migraine [70]. We assessed cutaneous allodynia in CD1 mice at P72-79 by measuring mechanical sensitivity on the plantar surface of the hindpaw using the von Frey test. We log-transformed the data and utilized a mixed-effects analysis followed by Bonferroni's multiple comparisons post-hoc test. The interaction between early life stress and treatment was significant ($p<0.001$). Both Control-CGRP ($p <0.001$, $t(94) = 5.92$) and ELS-CGRP treated mice ($p<0.001$, $t(94) = 8.18$) exhibited increased mechanical sensitivity (50% threshold) compared to baseline

sensitivity thresholds (Figure 6C). Neither the Control-Veh ($p = 0.08$, $t(94) = 1.80$) or ELS-Veh ($p = 0.16$, $t(94) = 1.41$) groups exhibited significant differences in sensitivity thresholds, as expected.

Light aversion or sensitivity to light is present in nearly all patients with migraine, and about 49% of patients reported photophobia (light aversion) as the most bothersome symptom of migraine [71]. At P81-85, we injected CGRP or PBS 30 minutes prior to placing animals into a light/dark box to assess light aversive behavior. Light aversion was measured by the average amount of time spent in the light zone of the light/dark box during the first 15 minutes of the testing period (Figure 6D). Using a Two-way ANOVA followed by Bonferroni's multiple comparisons post-hoc test, we found that the interaction between early life stress and treatment was significant ($p<0.0001$, $F(3, 93) = 7.90$). CGRP-treated control animals spent less time in the light following CGRP compared to PBS ($p<0.001$, $t (93) = 4.55$). CGRP-treated control animals also spent less time in light following CGRP compared to PBS ($p<0.001$, $t(93) = 5.18$). As expected, both Control-Veh ($p = 0.74$, $t(93) = 0.337$ and ELS-Veh ($p = 0.78$, $t(93) = 0.283$) did not show significant differences in time spent in light. Because the light/dark test can also be used to assess anxiety-like behavior, the standard in the field is to run an open field test under the same conditions as the light/dark test [72]. We tested the animals at P83-86. We found that there were no significant differences in time spent in the center during the open field test ($p= 0.76$, $F(3, 97) = 0.394$) (Figure 6E) thus leading us to conclude that CGRP-treated animals exhibited light aversion, and not anxiety-like behavior during the light/dark test. Overall, we found that ELS predisposes CD1 mice to enhanced peripheral CGRP-induced migraine-related phenotypes.

ELS induces changes in LFP power and coherence in response to CGRP

Having identified a relationship in which ELS predisposes CD1 mice to stronger migraine-like responses, we next set out to examine the impact of ELS on CGRP-response brain network responses. Given the role of the CeA in stress and affect and the changes in LFP power and coherence we observed, we

hypothesized that animals exposed to ELS would exhibit significant differences in LFP power in the CeA and CeA-related coherence in response to CGRP, compared to animals that remained group-housed during early life. ELS and group-housed control animals were treated with vehicle on Days 1 and 3, and CGRP on Day 2. We examined whether there was a significant interaction between ELS and CGRP response across time in these groups, as well as network-wide impacts of ELS itself in the absence of CGRP. We found significant differences in LFP power in response to CGRP between ELS and group-housed (control) mice in both the 4-7 Hz and 8-13 Hz across all brain regions of the network (i.e., a significant interaction, Figure 6F, Supplemental Figure S8-9) frequency bands. Overall, the ELS-CGRP group exhibited the strongest decrease from baseline of relative power and coherence across regions and pairings and the greatest amount of changes compared to control groups (ELS-vehicle, Control-vehicle, Control-CGRP) (Figure 6F).

Significant differences in LFP power were observed across all regions between ELS and control animals following CGRP administration, particularly in the 8-13 Hz frequency band (Figure 6F), however, there was largely no significant effect of ELS alone (Supplemental Figure S10). ELS animals showed a greater drop in LFP power in response to CGRP in both the CeA and Po with peak relative differences of 0.08 in the CeA (ELS x CGRP interaction p= 3.77e-16, ELS effect p= 0.11 , Figure 6G) and 0.10 in the Po (ELS x CGRP interaction p= 3.77e-16), ELS effect p= 0.22, Figure 6H) on the CGRP day.

Given the differences in power reactivities with ELS across both the CeA and Po, we examined whether coherence patterns in the Parabrachial-Amygdala-Thalamic subnetwork were also impacted (Figure 6I). Many significant differences in coherence were observed between control and ELS groups after CGRP administration, including Po-related pairings, which were consistently altered. Specifically, coherence was most disrupted in the ELS group in response to CGRP for the CeA-Po (ELS x CGRP interaction p= 3.77e-16, ELS effect p= 0.30, Figure 6J) and BLA-Po (ELS x CGRP interaction p= 7.04e-14, ELS effect p= 0.32, Figure 6K) pairings (see also Supplemental Figure S8-10). The ELS group also exhibited disrupted

coherence between LPBN-Po in response to CGRP (ELS x CGRP interaction p= 5.49e-5, ELS effect p= 0.65, Figure 6L).

Overall, these findings indicate that ELS induces changes in CeA and Po-related brain circuits in the context of CGRP, but not at baseline suggesting ELS sensitizes the brain's responsiveness to CGRP. Relative differences in mean log power with ELS were greatest in the BLA, CeA, and Po. Po-related brain region pairings showed the most significant coherence changes following CGRP administration, highlighting the importance of the Po in migraine-related brain circuitry following ELS exposure. These results are particularly intriguing in light of known CGRP-expressing pain pathways, wherein information from the parabrachial nuclei is sent to the amygdala or thalamic nuclei, which in turn relay signals to the amygdala or cortical regions [73]. Our data demonstrate that ELS predisposes mice to a migraine-susceptible brain state, resulting in compromised Po-related brain circuitry within CGRP-expressing pain pathways in the presence of CGRP. Such findings establish a novel model that predisposes rodents to a migraine-susceptible state (behaviorally and neurophysiologically), enabling rigorous investigation of dysfunctional migraine-related circuitry and providing a model for further evaluating central responses to CGRP.

Changepoint Analysis identifies differing brain network responses to peripherally delivered CGRP

Up to this point, we have provided a thorough demonstration of changes in brain activity over time with peripheral induction of CGRP across brain regions including with use of a common migraine-reducing drug and a naturally-occurring stressor that predisposes humans to migraine, early life stress. In order to identify the evolution of important network-wide events in the CGRP-induction of a migraine-like state, we employed a change-point analysis. This spectral-based method is used for detecting changes in the correlation structure of specific frequency components in the LFP (time series), over time, and the "principal component" of the LFPs, along which a change occurs. The change-point detection identifies

the epochs (i.e. the change points) across which a data-driven linear combination of the periodic components of LFP in our frequency bands of interest undergo a variance change. Thus, a changepoint reflects a point where coherence across multiple brain regions have a coordinated and significant change. We reasoned that the first changepoint after the injection is likely to be the most informative, as this likely reflects an animal's initial CNS response to the peripheral CGRP. The first changepoint after the injection (at 30 min), occurred within 40 minutes post-injection across all three days with no obvious relationship between light aversion behaviors and the timing of the first changepoint (Figure 7A). It does seem, however, that the time intervals between the change point and injection are smaller on day 2, the day CGRP was injected, than the vehicle days, 1 and 3. In order to ensure robustness of these findings, an additional robustness step was implemented, where we repeated the change point detection algorithm 50 times with different initialization random seeds, and evaluated the output change point locations by the mode and the projections by the median.

For a given changepoint, there exists a coefficient "projection" vector describing the brain region relationships that characterize the changepoint, which could be due to an altered synchronization strength among those brain regions in a given frequency band (see Fig. 7 and below). In order to determine whether there are common features regarding connectivity changes at the changepoint across animals in response to CGRP, we conducted a clustering analysis of the mice. We clustered in an unsupervised way based on the LFP features involved in each animals' changepoint, by using a cosine distance between the projection vectors of the mice. We reasoned that different CD1 mice might respond differently at the level of the CNS in response to peripheral CGRP (i.e. have different projections at the first change point) and we therefore used a k-medoids clustering approach to identify groups of mice that respond with similar projections. We used a silhouette coefficient to assess the strength of the clustering structure with average silhouette width >0.7 for each frequency (4-7Hz and 8-13 Hz). We

found six clusters this way, suggesting different brain network activity responses to CGRP in the CD1 mouse brain (Fig. 7B).

In order to understand the functional differences in the nature of changes in connectivity associated with these six different types of changepoints, we plotted the projection vectors for all of the animals grouped by cluster and ordered them from groups that are most to least photophobic in response to CGRP (Fig. 7 C,D). As shown in Figure 7C, different coherency organizational structures, as indicated by the projection vectors (see Methods), define groups that are more or less susceptible to the migraine-inducing effects of peripheral CGRP injection. In other words, the network activity around the first changepoint explains the behavioral phenotype. To quantify the extent to which network activity can be used to predict hypersusceptibility to migraine in the mice, we calculated an AUC for the most highly susceptible group containing at least three animal compared to the rest of the animals for 4-7Hz and 8-13Hz (AUC=0.95, p=0.006 4-7Hz; AUC=0.72, p=0.188, 8-13 Hz). In order to assess whether this relationship between brain network activity and behavior was specific for CGRP we did the same comparison for days 1 and 3 and found much weaker associations with behavior (day 1 AUC=0.48, p=0.95, day 3 AUC=0.61,p=0.488, 4-7Hz; day1 AUC=0.55, p=0.650, day3 AUC=0.54,p=0.658, 8-13 Hz). Altogether, these data demonstrate that there is not one global response in connectivity of all animals to CGRP, and that coherence changes at the first timepoint following CGRP injection can be used to predict animals with extreme migraine-like response.

In order to provide a more direct biological interpretation of the network features defining this network of migraine hypersusceptibility, we examined the coherency matrices immediately before and immediately following the changepoint (Supplemental Fig. S12-S14). In Figure 7E, we show the cluster mean of difference of coherency matrix on 4-7 Hz over the first change point after injection (in clusters with at least three mice and ordered by the average relative dark ratio, 8-13Hz in Supplemental Figure S12). For the 4-7 Hz frequency band, clear block-wise structure is observed for cluster 1, 3 and 4 (cluster

1 in the 8-13 Hz band). Interestingly, cluster 1, the cluster in which the animals have the most photophobic response to CGRP, is the only cluster in which coherence is increased at the first changepoint following CGRP injection. This is consistent with the idea of the migraine response being concerted across multiple synchronized brain regions during specific events, while desynchronizing networks overall. In particular, it seems to be the parabrachial nuclei, which have CGRP projections and receive projections from the trigeminal input as well as the ACC, which is heavily involved in the emotional response to pain, that seem to be at the center of this increased synchrony. Animals with the least photophobic response to CGRP have a less block-wise structure with minor decreases in coherence between the PBN and emotional pain regions (Amygdalar nuclei and ACC). The 4-7 Hz connectivity patterns continue to reflect interesting relationships with behavior, as the next two most photosensitive groups of animals (clusters 5 and 3) had depressed synchrony between the PBN regions (left and right) and the remaining six regions, and otherwise little to no changes. The connectivity patterns in cluster 2 suggest suppressed between-group synchrony among three groups of nuclei, namely, the PBNs, the thalamic nuclei, and amygdala nuclei and ACC being the third group, while there were little to no within group changes. Cluster 4 had different connectivity patterns showing depressed between-group synchrony with the PBNs and the thalamic nuclei forming a group while the amygdala nuclei and ACC as the second group. When thalamic nuclei change in the same direction as the PBNs as in clusters 2 and 4, photophobia tends to be much lower. In the 8-13 Hz range we see a similar, but slightly different connectivity relationship with behavior (Supplemental Fig. S11). There is no single rule that applies to all of the animals in the top three groups, but the trend is again that the PBNs act together as a group while the thalamic and amygdalar nuclei act as another distinct group, with elevated or suppressed between-group synchrony by CGRP. Clusters 2 and 4 again for the largest distinct groups having two predominating responses to CGRP and demonstrating the least photosensitivity (Fig. 7E). Furthermore, we showed the differences of the post- from the pre-change-point pairwise correlations between the

eight brain regions, per mouse (Supplemental Fig. S13) and the mean differences per cluster (Fig. 7E and Supplemental Fig. S12.

Discussion

Migraine is a complex and profound disorder, which includes experiences of pain and episodic disabling brain function, impacting up to 20% of the population at some point (~1 billion people worldwide). A disorder which induces systemic and coordinated malfunction of brain systems spanning emotion, sensation, autonomic nervous system regulation, and cognition, begs for a systems neuroscience approach [30]. The field's understanding of migraine has evolved significantly, shifting from thinking of it as a primarily neurovascular disorder to a complex neurological condition involving multiple brain regions, with different regions engaged during distinct phases [74,75] . The complexity of migraine pathophysiology is underscored by the fact that the underlying neuronal mechanisms of migraine have remained a major open question in the field [30]. Several evidences point toward both central and peripheral pathophysiology, including the complex symptomatology experienced by patients with migraine, differences in functional connectivity between patients and healthy controls, and varied pharmacological responses; how exactly brain networks coordinate over time to produce a migraine brain state remain unknown. In this study, we have implemented a systems-based approach combining multi-site in vivo neurophysiology with peripheral CGRP injection, migraine-relevant behavioral assays, sumatriptan treatment and early life stress to report on the underlying central mechanisms of a peripherally induced migraine brain state.

Overall, CGRP injection provides a robust preclinical model to investigate mechanisms underlying the complex symptomatology and pathophysiology of migraine, and a path by which we can precisely characterize features of the migraine brain state. CGRP as a mouse model of migraine has face [31], predictive [76,77], and construct validity [31,77] , which is the primary target of recent major migraine

therapeutics [78,79]. While early studies have shown a clear peripheral role of CGRP in migraine, the field has likely only scratched the surface of uncovering its central actions.

Nociceptive primary afferents carrying CGRP provide input to second-order neurons of the spinal dorsal horn and trigeminal nucleus caudalis [24,80]. These second-order neuronal projections then transmit nociceptive input to the parabrachial and thalamic nuclei. There also exists a monosynaptic connection including CGRP-expressing neurons between trigeminal afferents and the parabrachial nucleus, which has been shown to transduce craniofacial affective pain [28]. Significantly, this direct connection has been found in the dura, a key anatomical substrate in migraine pain [81]. CGRP has been found in projections from parabrachial neurons to the thalamus and amygdala [73]. CGRP can also directly or indirectly modulate neuronal activity and synaptic plasticity in several brain regions implicated in migraine, including the cortex, amygdala and thalamus [73,82,83]. These findings suggest that CGRP may disrupt normal brain network dynamics and contribute to the generation of migraine headaches and its associated symptoms. These data all contribute to our hypothesis that peripheral CGRP facilitates nociceptive transmission into the cortex and contributes to the sensitization of both primary afferent sensory and second-order pain neurons to evoke at least part of the migraine brain state.

Here, we have identified a peripheral CGRP-induced migraine brain state characterized by directional circuitry, changes in LFP power across time in two different frequency bands, and coherence disruption within these frequency bands across brain region pairings (Figure 8). Quantifying spatiotemporal dynamics following peripheral CGRP administration based on LFP activity, we demonstrate how coordinated brain-wide network activity over time mediates several aspects of migraine and underscore the importance of a systems-level approach to migraine research.

The changes in power and coherence following CGRP injection, and under different conditions, are particularly interesting when considering the time course of changes in the context of migraine as a

phasic disorder. In the 4-7 Hz range, we found that CGRP injection led to a decrease in power across all 8 regions which peaked at 10-30 minutes post-injection, primarily resolved by 45 minutes post-injection, and resolved completely by ~60 minutes post-injection (Fig 3). A similar time course of CGRP-induced behavioral sensitization was found in a study where peripherally administered CGRP induced a significantly greater spontaneous facial pain response than controls starting 10 min post-injection, peaking at 30 minutes, and lasting for about 75-90 minutes [55]. This time course of CGRP-induced migraine phenotype is consistent with other preclinical mouse models of migraine, and, to some extent, human studies of photophobia [32,84]. However, coherence holistically followed a different (shorter) time course. Significant disruptions in coherence among brain region pairings were especially prevalent in the first 10 minutes immediately post–injection of CGRP, and resolved around 20 minutes post-injection. This time course of CGRP-induced changes in coherence gives us insight into how information flow between brain regions is disrupted by a migraine trigger or early in a migraine attack to orchestrate the migraine brain state. Because CGRP enhances sensitivity to sensory input in both the periphery and central nervous system, it is possible the changes in coherence are a reflection of a transition into a hypersensitized brain state [85].

Sumatriptan is a triptan class of 5-$HT_{1B/1D}$ receptor agonists, which are well-established therapeutics for migraine [86]. While born out of the vascular hypothesis of migraine, research suggests that central action can be attributed to the efficacy of sumatriptan in migraine treatment, though the exact site of action remains elusive and its ability to penetrate the blood-brain barrier remains a debate [59,61,87,88]. Importantly, sumatriptan can directly repress the migraine-related increase in CGRP secretion from trigeminal neurons and normalize cranial CGRP levels[87]. Thus, we hypothesized that coadministration of CGRP and sumatriptan would attenuate some or all of the changes in power and coherence induced by CGRP. Coadministration of CGRP and sumatriptan reversed the changes in power in the ACC, BLA, and CeA in the 8-13 Hz frequency band especially at 25 minutes post-injection. Our coherence findings

showed that coadministration reversed coherence disruptions in brain region pairings involving the BLA and ACC, especially within the first 20 minutes post-injection. This indicates that sumatriptan exerts its effects on coherence most prominently during the early phase of interaction between cortical and subcortical regions. Interestingly, an fMRI study with normal, healthy volunteers showed that CGRP increased BOLD-signal in the brainstem and insula and decreased BOLD-signal in the caudate nuclei, thalamus, and cingulate cortex in response to a noxious stimulus [89]. These changes in BOLD-signal are reversed by sumatriptan at 40 minutes post-CGRP injection and 15 minutes post-sumatriptan injection. Although we did not observe the most significant changes in the brain region pairings most disrupted in response to CGRP (except BLA-VPM), one possible limitation of our study is that we did not administer a drug that acts directly on CGRP. Future studies should investigate the effect of CGRP-targeting pharmacologics (e.g., CGRP monoclonal antibodies, CGRP antagonists) on CGRP-induced brain states to assess whether network activity is more strongly attenuated. Our sumatriptan experiments are a first step in investigating whether common migraine drugs reduce the brain network activity associated with susceptibility. Overall, our sumatriptan and CGRP coadministration findings show that sumatriptan reverses some power and coherence changes induced by CGRP, at least in circuits involving the ACC and amygdala..

Stress is a common trigger for migraine, high levels of stress are reported in migraine patients and, simultaneously, migraine is comorbid with numerous brain disorders associated with stress, making this an important association to uncover [90]. Critically, stress physiologically increases susceptibility to migraine, but the mechanisms by which stress contributes to migraine are poorly understood [91]. Restraint stress has been shown to produce significant facial hypersensitivity in mice, causing priming to a subthreshold dose of the NO-donor sodium nitroprusside, and responses to this priming were blocked by CGRP monoclonal antibody [92]. ELS has a well-documented association with migraine and headache in adulthood, with the number of stressors increasing risk [80]. A study using maternal separation in rats and

induced chronic migraine using the migraine-inducing compound NTG, a nitric oxide donor, found significant differences in migraine-related behavior between the ELS rats and controls [68]. Additionally, a study using C57Bl/6 mice demonstrated that female mice that had undergone maternal separation stress in early life exhibited increased migraine-related mechanical sensitivity, spontaneous pain and light aversion compared to controls following NTG administration [69]. Both studies demonstrated significant differences in migraine-like phenotypes following ELS in female rodents, which mirrors findings in human literature [93]. However, up to this point, ELS had not yet been investigated in a CD1 mouse strain or CGRP mouse model of migraine. Thus, in addition to characterizing a CGRP-induced migraine brain state, we utilized ELS to investigate the relationship between stress and migraine in the context of CGRP. ELS mice exhibited increased anxiety-like behavior, increased mechanical allodynia, and decreased time spent in light independent of anxiety with enhanced responses compared to controls in response to CGRP. In response to CGRP, ELS significantly enhanced the drop in power found in the CeA and Po, and the peak relative differences occurred near the middle of the analysis period. Coherence patterns between Po-related brain circuits were more disrupted in ELS animals compared to controls. Additionally, while coherence was most disrupted between the PBN and CeA in our CGRP experiments, the coherence between this pairing resolved around 20 minutes post-injection. In ELS animals, however, coherence between Po-related circuits took longer to resolved, occurring at ~30 minutes post-injection. Altogether, these findings indicate that ELS is able to induce changes in network activity of CeA and Po-related brain circuits when sensitized to CGRP. The relative differences in mean log power and mean log-odds coherence are greatest in the Po and Po-related brain pairings, supporting the importance of this region in ELS-related brain circuitry. As migraine disproportionately effects women, and ELS has been shown to induce different brain and behavior responses in males and females, future studies to further probe this relationship are needed [94]. Finally, given the pain pathways where CGRP is expressed by which information from the parabrachial nuclei is sent to the amygdala or

thalamic nuclei and thalamic nuclei send information to cortical regions, our data demonstrate that ELS may lead to vulnerability to changes in Po-related brain circuitry in CGRP-expressing pain pathways and subsequently susceptibility to migraine.

These global findings provide an overall picture of brain network responses generalized across the population that we measured, however, our changepoint analysis best help us understand what brain network activity might be most contributing to individualized migraine-like responses. Given the heterogeneity of migraine experience, we thought this was especially important to pursue.

We identified changepoints, which are time epochs where LFP signals within specific frequency bands undergo a substantial and coordinated change in variance. Our change-point analysis clusters suggest different brain network activity responses to CGRP in the CD1 mouse brain. These clusters, when ordered from most to least photophobic in response to CGRP, revealed different coherency organizational structures which defined groups that are more or less susceptible to peripheral CGRP injection-induced migraine. Importantly, the network activity around the first changepoint – 10 minutes post-injection – provides sufficient information to explain or even to some extent predict, the behavioral phenotype. Thus, coherence changes at this first timepoint following CGRP injection can be used to predict animals with extreme migraine-like response to light. Interestingly, the cluster of animals with the most photophobic response to CGRP are the only cluster in which coherence in the 4-7 Hz frequency range is increased at the first changepoint. Specifically, the parabrachial nuclei and ACC seem to be at the center of this synchrony. Our change-point analysis clusters revealed how differences in brain network activity responses to CGRP reflect differences in migraine-related behaviors in response to CGRP. Pinpointing the differences between migraine susceptible and resilient brain network activity open up exciting possibilities in migraine treatment.

Our findings on the timing differences in coherence and power changes across conditions give us insight into how the migraine brain state develops over time to produce phase-dependent symptomology. Furthermore, these differences reflect the cyclical nature of migraine, with external stimuli represented by the different conditions impacting when and how these changes occur in response to CGRP. Findings from our coadministration of sumatriptan and CGRP experiments are a first step in investigating whether common migraine drugs reverse the brain network activity associated with susceptibility. Our ELS experiments show how the migraine brain state may be primed by stress in early life and underscore the need for additional studies on the interaction between sex and migraine. Our results provide unique insights into the neural basis of migraine and may have implications for the development of novel therapies targeting brain-wide networks or modulation of different brain regions.

Figure Legends

Figure 1. Peripheral injection of CGRP induces light-aversive behavior in electrode-implanted animals Mice were placed in a light/dark box for a total of 30 minutes to assess light aversive behavior indicated by total time spent in the light zone in response to PBS (vehicle) and CGRP. A) Histological verification of 34 CD1 mice (16 M, 18 F) implanted with metal wires in the anterior cingulate cortex, basolateral amygdala, central amygdala, ventroposteromedial thalamus, mediodorsal thalamus, posterior thalamus, and bilateral parabrachial nuclei. B) Experimental timeline of recordings and behavior. C) Experimental paradigm of the light/dark test of light aversion utilized. D) Unimplanted (n= 7) and electrode-implanted (n= 7) CD1 mice exhibit light aversive behavior in response to CGRP, and the treatment interaction between the treatment and electrode-implanted condition was not significant. E) A subset of unimplanted mice demonstrate no difference in time spent in light when treated with PBS (n= 5) on the treatment day, while CGRP-treated mice exhibit decreased time spent in light (n= 7). Data are represented as mean ± SEM.

Figure 2. LFP directionality between the mediodorsal thalamus, posterior thalamus, ventroposteromedial thalamus, central amygdala, and parabrachial nuclei is the greatest at the 4-7 and 8-13 Hz frequency bands. The offset at which each pair of LFPs optimally phase synchronized is plotted for each frequency +/- SEM.A-E) The mean temporal offset across the MD, Po, VPM, CeA, and PBN pairings are the greatest in the 1-3 Hz (green), 4-7 Hz (orange), and 8-13 Hz (purple) frequency bands indicated by the dashed lines. The solid purple lines indicated the mean temporal offset at

frequency bands 1-50 Hz. Each shaded purple area represents standard deviation from the mean (1-3 standard deviations). F) Summarized directionality relationships across all regions.

Figure 3. CGRP induces LFP power differences in the 4-7 Hz frequency band. A) Representative spectral power plot of the Acc across 1-13 Hz. Power is represented in decibels (dB). (left) Heat map showing all p-values across brain regions of interest. (right) B-H) Plot showing the mean log-power across time following CGRP treatment (pink) compared to vehicle PBS (blue) (left). Function on scalar generalized additive model analysis (FOS) plot showing the difference between the mean log-power when animals were treated with CGRP and PBS across time immediately post-injection. Data are represented as 30-second rolling means ± SEM.

Figure 4. CGRP induces disruptions in LFP coherence across migraine-related brain regions. A) High mean coherence was observed during the 1-13 Hz frequency range. B) Representative coherence plot of the CeA-LPBN and CeA-Po across 1-13 Hz. Red arrow indicates injection point.C) Heat map showing the difference between CGRP and vehicle mean log-odds coherence. D-F) The CeA-LPBN, CeA-Po, and BLA-VPM pairings showed the greatest differences in mean log-odds coherence in response to CGRP compared to vehicle. Coherence was partially disrupted between the LPBN-Po (G), ACC-BLA (H), and ACC-CeA (I). Data are represented as 30-second rolling means ± SEM.

Figure 5. Coadministration of CGRP and Sumatriptan partially reverses the effect of CGRP. A) Experimental timeline of sumatriptan and CGRP experiments. B) Heat map showing -log10 p-values summarizing the effect of sumatriptan+CGRP on LFP power and coherence (F). Red boxes indicate significant differences in which reversal of the CGRP effect occurred. C-E) Sumatriptan+CGRP reverses the effect of CGRP alone on LFP power in the ACC, BLA, and CeA. G-K) Sumatriptan+CGRP reversed the disruption in coherence between the CeA-LPBN, CeA-Po, BLA-VPM, ACC-BLA, and ACC-CeA. (n= 10) Power data are represented as 30-second rolling means ± SEM. Coherence data are represented as 60-second rolling means ± SEM.

Figure 6. ELS exacerbates migraine-related behavior and alters CeA and Po-related circuitry in the presence of CGRP. Animals underwent maternal separation stress and migraine-related behavior was measured. A) Timeline of ELS experiment with behavior and recordings. (n= Control Veh:24, Control-CGRP: 24, ELS-Veh: 28, ELS-CGRP: 27) B) Animals spend less time in the open arms of the elevated plus maze following ELS C) CGRP-treated animals exhibit increased 50% threshold compared to baseline. D) CGRP-treated animals spend less time in the light during the light/dark assay. E) There were no significant differences in time spent in the center of the open field test following the light/dark assay. F) Heat map of -log10 p-values reflecting the interaction between ELS x CGRP in ELS compared to control mice effect on LFP power and coherence (I). G-H) ELS-CGRP mice showed the greatest changes in LFP power in the CeA and Po (n=11). J-L) Coherence was disrupted the most in Po-related circuits. Power data are represented as 30-second rolling means mean ± SEM. Coherence data are represented as 60-second rolling means ± SEM.

Figure 7. Changepoint Analysis identifies differing brain network responses to peripherally delivered CGRP. A) Time of 1st change point after injection (at 30min) is shown on the y-axis, and mice are shown in decreasing order of their behavior in order from greatest to least photophobia following CGRP B) 4-7Hz k-medoids clustering of initial changepoint projection features following injection with CGRP, silhouette width on the x axis, and each mouse on the y axis, the counts and average silhouette width in

each cluster listed on the right, and the overall average silhouette width on the bottom. C) 4-7Hz projection features for each mouse by cluster (colors to left). Brain regions are represented across the bottom with each mouse representing a different row, ordered by the cluster average of highest relative dark ratio (most photophobic) at the top. The legend shows the color of values of each cluster in the heatmap. D) 4-7 Hz relationship between brain network feature clustering and behavior on the light/dark test, represented by the relative dark ratio= Treatment time in dark/ Vehicle time in dark. E) The cluster mean of difference of coherency matrix for 4-7 Hz over the first change point (i.e. the change in coherency matrices from the segment preceding changepoint to the segment after changepoint) after injection (in clusters with at least 3 mice and ordered by the average relative dark ratio) .

Figure 8. Model of Migraine Network Activity. Top: Brain network components implicated in migraine either by human fMRI or by rodent pain studies. Bottom: Model of brain network activity in peripheral CGRP-induced migraine state.

EXPERIMENTAL MODEL AND STUDY PARTICIPANT DETAILS

Animal Care and Use

All experiments were performed with approved protocols by the Institutional Animal Care and Use Committee (IACUC) of the University of Iowa. CD1 mice purchased from Charles River Laboratory were utilized for all experiments. For neurophysiological experiments (excluding maternal separation stress), male and female mice aged 9 weeks of age were group housed 2-3 animals per cage for 1 week prior to surgery. Mice were maintained on a 12 h light/dark cycle with ad libitum access to food and water. All testing was performed between 9:00 AM and 9:00 PM.

Maternal Separation Stress with Early Weaning and Limited Nesting

CD1 mice were obtained from Charles River Laboratory and bred in-house to generate breeding pairs and their offspring. All experimental animals were a minimum of one generation removed from shipping stress. Behavioral testing was conducted across several cohorts based on parturition date. The maternal separation stress paradigm was adapted from previously described methods [95,96]. All mice were housed on beta chip bedding with only 1/3 of the supplemental nesting material provided to controls (Enviro-Dri

nesting material). Litters were culled to 8 pups on P1 with balanced sex distribution. Starting at P2, pups were separated from dams for 4 hours daily until P5 then 8 hours daily until P16. Supplemental heat was provided during separation periods. Pups were weaned early at P17 to eliminate the likelihood of overcompensation of maternal care behavior upon dams reunion with pups [97]. Prior to experiments, animals were weighed weekly and placed into balanced treatment groups based on weights and cohort.

METHOD DETAILS

Neurophysiological Experiments

Drug Administration

All injections were performed intraperitoneally (IP) with a 25G needle. We administered calcitonin gene-related peptide (CGRP) (Sigma-Aldrich, Saint Louis, MO) at 0.1 mg/kg and sumatriptan at 0.6 mg/kg (AuroMedics Pharma LLC, E. Windsor, NJ). We utilized phosphate-buffered saline (PBS) as a diluent and vehicle for all experiments. We co-injected sumatriptan and CGRP by doubling the total volumes of each and diluting them such that our co-injections were the same solution volume as the single CGRP and PBS injections. All solutions were prepared 1 hour prior to the start of experiments and placed on ice for the remainder of the experiment.

Electrode Implantation

Animals aged 10-12 weeks were anesthetized with isoflurane, placed in a stereotaxic device, and craniotomized for electrode implantation. Metal ground screws were secured above the olfactory bulb and cerebellum. Tungsten wires (California Fine Wires) were implanted in the anterior cingulate cortex (ACC), ventral posteromedial thalamus (VPM), medial dorsal thalamus (MDthal), posterior thalamus (Po), central amygdala (CeA), basolateral amygdala (BLA), and left and right parabrachial nucleus

(LPBN/RPBN). Coordinates were adapted for CD1 animals and verified histologically. Male surgical coordinates for the center of bundles placed (not actual electrode tips) are as follows: ACC, 0.8mm A/P, 0.25mm M/L, 1.8mm D/V; Amy (BLA/CeA) -1.58mm A/P, 2.75mm M/L, 3.9mm D/V; thal (MDthal/Po/VPM) -1.82mm A/P, 1.5mm M/L, 3.1mm D/V; PBN -5.5mm A/P, +/-1.5mm M/L, 2.3mm D/V. Female are: 0.78mm A/P, 0.24mm M/L, 1.8mm D/V; Amy (BLA/CeA) -1.54mm A/P, 2.68mm M/L, 3.8mm D/V, thal (MDthal/Po/VPM) -1.77mm A/P, 1.46mm M/L, 3.02mm D/V; PBN -5.36mm A/P, +/-1.46mm M/L, 2.24mm D/V.

Light-Aversion Test

To assess light-aversive behavior, we performed a light/dark assay. In this assay, animals were placed in a transparent testing chamber (MedAssociates, East Fairfield, VT) consisting of a dark or light zone divided by a dark insert. We utilized infrared beam tracking and Activity Monitor software to analyze activity across a 30-minute time period under 20,000 lux light intensity. On the first day, animals underwent a baseline assessment in which they are placed in the testing chamber for a 30-minute period. Mice were injected with vehicle the following day and assessed for another 30-minute period. Lastly, animals were injected with CGRP and activity was monitored for 30 minutes in the testing chamber. For ELS experiments, testing occurred at P81-85.

Neurophysiological recordings

Mice were connected to Mu headstages (Blackrock Microsystems, UT, USA) under isoflurane anesthesia prior to recordings. During recordings, mice were placed in a homecage environment consisting of standard cages with corn cob bedding and recorded for 30 minutes under baseline conditions. Neurophysiological data was captured using the Cereplex Direct acquisition system and sampled at 30kHz. Local field potentials (LFPs) were stored at 1000 Hz and a bandpass filter was applied at 0.5-250 Hz.

Timeline of neurophysiological recordings during peripheral administration of CGRP

Two weeks following recovery from surgery, animals underwent three days of homecage recordings. On Day 1, animals were recorded for 30 minutes then received an IP PBS vehicle injection and recorded for an additional 2 hours post-injection. Day 2, we administered IP CGRP injections. To ensure any observed changes in brain activity on Day 2 could be attributed to changes induced by CGRP and not the injection itself, we injected animals with PBS.

Histology/Electrode Placement

All animals were euthanized upon completion of experiments and perfused with 4% paraformaldehyde (PFA). Brains were stored in 30% sucrose overnight and submerged in an OCT compound then frozen on dry ice and stored at -80°C. Brains were sliced in 35µm sections then washed in PBS prior to being stained with red Nissl (ThermoFisher, Waltham, MA). Slices were imaged at 5x magnification using a Leica fluorescence microscope. Each individual slice was aligned to the Paxinos and Franklin brain atlas for verification of electrode placement.

Early Life Stress Behavioral Experiments

Elevated Plus Maze

To assess anxiety-like behavior in mice, we utilized an elevated plus maze (EPM) apparatus consisting of two opposing open and closed arms. A video camera was placed directly above the center of the maze to capture activity during each trial. Each animal was placed in the center of the EPM facing the same closed arm at the start of each trial and tested for a total of 5 minutes. All mice were tested at P66-69.

Plantar von Frey Test

To assess mechanical allodynia in mice, we utilized the plantar von Frey test. Over a total of 5 days, mice were placed in acrylic chambers over a grid support (Bioseb, France). Mice habituated to the chambers for a total of 2 hours the first two days. For each of the following days, mice habituated to the chambers for 1 hour prior to the start of experiments. Mice were considered well habituated when standing on all four paws, calm, and non-responsive to the habituation filament . Starting on Day 3 (Baseline day), a von Frey filament was applied to the plantar surface of the right hindpaw. We followed the "up-down" method to obtain a paw withdrawal threshold for each animal [98,99]. On Day 4, all animals received an IP PBS (vehicle) injection and were allowed to rest for 30 minutes prior to testing. On Day 5, animals received either CGRP or vehicle injections and were allowed to rest for 30 minutes prior to testing. Animals were tested at P72-79.

Open Field Test

To determine whether the light aversive behavior was independent of anxiety-like behavior in mice, we performed an open field test. Animals were tested at the end of the experiments at P83-86 the day after light aversion experiments. Mice were placed in a large open field box for 20 minutes at a time following administration of vehicle and CGRP. We utilized ANY-maze software to monitor the total amount of time animals spent in the center zone of the open field box.

QUANTIFICATION AND STATISTICAL ANALYSIS

Implanted vs. Unimplanted Behavioral Statistics

We fit a three factor mixed effects model using the *lme4 R* library [100] with fixed effects terms for the model intercept, CGRP, day, implant and the interaction between CGRP and implant. We employed a

random intercept for each mouse. We obtained the reported p-values for the fixed effects terms using the *lmerTest R* library [101].

Directionality Analysis

LFP signal directionality between pairs of brain regions was estimated using a temporal lag approach introducing phase offsets as previously described [40]. Butterworth bandpass filters were applied to isolate LFP oscillations within 1Hz windows using a 1Hz step in the 1-50Hz range. The Hilbert transform was used to determine the instantaneous phase of the filtered LFPs and the instantaneous phase offset time series was calculated for each LFP brain region pair. The mean resultant length (MRL) for the phase offset time series was calculated, yielding the phase coherence between pairs of LFPs. Temporal offsets were introduced between each pair of LFPs ranging from -250ms to 250ms in 2 ms steps and the phase coherence was recalculated between each LFP pair.

Frequency Band Identification

In order to determine the specific frequency bands at which pairs of brain regions demonstrated clear temporal offset (leading or lagging), we used a fused lasso approach within the 1*Hz* to 50*Hz* range obtained from the phase offsets data for 34 mice and for each pair of brain regions from the set: ACC, LPBN, RPBN, CeA, BLA, MD_thal, Po, VPM. Lasso (Least absolute shrinkage and selection operator), is a model parameter selection and regularization method. The lasso method minimizes the least squares loss over a set of parameters in a linear regression problem by imposing the condition that the sum of the absolute values of the parameter estimates (that is, the ℓ_1 norm of the parameters) is less than some value [102]. This method generally results in some parameter estimates being zeroed out, in effect selecting the most important covariates that are more predictive of the response than those with zeroed out regression coefficients. The fused lasso accounts for temporal or spatial dependence amongst covariates by further imposing a condition that the sum of the absolute values of the lag one differences

between subsequent parameter estimates be less than some value [103]. Modeling the response under

$$\underset{\underline{\beta}\in\mathbb{R}^p}{\operatorname{argmin}}\|\underline{y}-X\underline{\beta}\|_2^2+\lambda\sum_{i=1}^{p}|\beta_i|+\gamma\sum_{j=2}^{p}|\beta_j-\beta_{j-1}|.$$

fused lasso then amounts to finding a set of parameter estimates $\hat{\underline{\beta}}\in\mathbb{R}^p$ as a solution of

The parameters λ and γ are positive tuning parameters. The solution of the optimization problem in (1) depends on the chosen value of λ and γ, that is $\hat{\underline{\beta}}_{\lambda,\gamma}$, which are chosen via cross validation in such a way that the test mean squared error is minimized.

We hypothesized that a small number of frequencies are active in these measurements and an active frequency implies that neighboring frequencies are also active. We applied the application of fused lasso for signal approximation [104]. We first computed the mean over all observations for each pair of brain regions and for each mouse. This resulted in 168 observations (8 mice times 21 brain region pairs) each with 50 elements corresponding to the mean phase offset at each frequency from 1*Hz* to 50*Hz*. This 168 × 50 matrix was then reshaped into a 400 × 21 response matrix **Y** in which each column contained the means across frequencies for each mouse for a particular pair of brain regions. The design matrix **X** was comprised of eight 50 × 50 identity matrices stacked on top of each other (one for each mouse) resulting in a 400 × 50 matrix. The $\hat{\boldsymbol{\beta}}$ matrix of parameter estimates was a 50 × 21 matrix for which each column contained the model estimates for the phase offsets over the 1*Hz* to 50*Hz* range for a given pair of brain regions. We then used the genlasso library (*genlasso: Path Algorithm for Generalized Lasso Problems* ,R package 1.5) in R to obtain estimates $\hat{\boldsymbol{\beta}}$ under the fused lasso model with the tuning parameters λ and γ set to 3 and 0.5 respectively. This resulted in 21 different vectors (the columns of $\hat{\underline{\beta}}$) with bands of non-zero values corresponding to significant phase offset frequencies and zeros indicating non-significant frequencies for each pair of brain regions.

Frequency bands of interest

The Po-CeA relationship was the only brain region pairing that included a different, 1-7 Hz band. We accounted for 1-3 Hz and 1-7 Hz in our multiple comparisons corrections, however we did not observe substantial evidence for the biological relevance of the 1-3 Hz band across all brain regions we observed given how small the differences in this band were relative to the other frequency bands and the fact that it was only significant in one region pairing and not all (Supplemental Figure S3) so we focused on the 4-7 Hz and 8-13 Hz frequency bands.

Analysis of Power and Coherence over time

We applied a log transformation to the recordings to preprocess the power data. For every brain region and every mouse on each day of the experiment, we averaged the log-transformed power across all channels within each brain region and all frequencies within specific frequency bands. This resulted in a single log-power time series for every frequency band and for every brain region being associated with each mouse on each day of an experiment. We computed the mean log-power over baseline recordings for each frequency band and brain region for each mouse on each day of a given experiment. We normalized the post-injection log-power recordings relative to the baseline by subtracting these means from the corresponding log-power post-injection recordings.

We preprocessed the coherence data similarly. For each pair of brain regions and all frequencies within specific frequency bands, the coherence recordings were averaged across all the channel pairs, resulting in a single coherence time series for every frequency band across each mouse's 28 pairs of brain regions on each day. We then applied a log-odds transformation to the averaged coherence data to normalize the post-injection log-odds coherence recordings using the same approach as we did for the power data. Specifically, we calculated the mean of the baseline log-odds coherence for each frequency band and

brain region pair and subtracted these means from the corresponding post-injection log-odds coherence values.

After preprocessing, we used these data to fit the FOS model using generalized additive model (GAM) function in the mgcv library in R to plot 30 second rolling means in order to identify underlying trends over time [105]. We first computed 30-second rolling means over each mouse's log-power post-injection time series for each day of the experiment, for each frequency band and each brain region, using the *tf_smooth* function in the *R* library *tf* [106]. Next, we averaged the vehicle 30-second rolling mean time series across days. This resulted in each mouse having one log-power 30 second rolling mean post-injection time series for each treatment (vehicle and CGRP), frequency band, and brain region. We used these series for all the mice to compute the average and one standard deviation and obtained one mean CGRP log-power time series, one mean vehicle log-power time series and their respective one standard deviation time series for each frequency band for each brain region. For each frequency band in each brain region, we plotted these 30-second rolling mean time series together to facilitate comparison between the CGRP and vehicle conditions. We used the *R* packages *ggplot2*[107] and *tidyfun*[106,108] to plot these figures.

We applied the same procedure to the coherence data, resulting in one mean CGRP log-odds coherence 30-second rolling mean time series, one mean vehicle log-odds coherence 30-second rolling mean time series, and their respective one standard deviation time series for each frequency band across each pair of brain regions. We plotted these 30 second rolling mean time series together for comparison in the same manner as the log-power analyses.

For the power GAM analysis, we computed the mean of each mouse's log-power post-injection vehicle time series, resulting in one log-power post-injection time series for vehicle and one for CGRP for each frequency band in each brain region. We obtained one pairwise difference time

series for each frequency band in each brain region for each mouse by subtracting the mouse's log-power vehicle time series from the corresponding CGRP time series. For each frequency band in each brain region, we used 90 minutes of the post-injection recordings for the power data analysis.

The coherence analysis is performed similarly, except we computed the mean log-odds coherence instead of the mean log-power. This resulted in each mouse having one log-odds coherence post-injection time series for the vehicle and one for CGRP for each frequency band across each pair of brain regions. We then subtracted each mouse's log-odds coherence vehicle time series from the corresponding CGRP time series to obtain one pairwise difference time series for each frequency band across each pair of brain regions for each mouse. For each frequency band in each brain region, we used 60 minutes of the post-injection recordings data for the coherence data analysis.

The coherence analysis is performed similarly, except we computed the mean log-odds coherence instead of the mean log-power. This resulted in each mouse having one log-odds coherence post-injection time series for the vehicle and one for CGRP for each frequency band across each pair of brain regions. We then subtracted each mouse's log-odds coherence vehicle time series from the corresponding CGRP time series to obtain one pairwise difference time series for each frequency band across each pair of brain regions for each mouse. For each frequency band in each brain region, we used 60 minutes of the post-injection recordings data for the coherence data analysis.

For the power and coherence analyses, we used the *gam* function in the *R* package *mgcv* (Wood, 2011) for FOS regression. Each model had the following form:

$$y_{r,f}(t) = \beta_{r,f} + s_{r,f}(t) + \varepsilon_{r,f}(t), \tag{1}$$

where $y_{r,f}(t)$ denotes the pairwise difference in log-power or log-odds coherence at time point *t,* brain region (for power) or pair of regions (for coherence) *r* and frequency band *f*; $\beta_{r,f}$ denotes the *(r, f)*-specific model intercept; $s_{r,f}(t)$ denotes the *(r, f)*-specific model smooth function-over-time effect at time point t; and $\varepsilon_{r,f}(t)$ denotes *(r, f)*-specific independent centered Gaussian noise at time point t. This FOS regression model assumes that the pairwise differences in log-power or log-odds coherence are frequency band and region- or pair-specific functions of time.

We fit this model in *R* as follows. For the mouse *i*, $X_{i,r,f}$ denotes the *R* data.frame with columns representing time and response, where *t* is the vector of evenly spaced time steps and y denotes the observed pairwise difference in log-power or log-odds coherence for mouse i in brain region or pair of brain regions *r* and frequency band *f*. Let *X_rf* denote the data.frame formed by stacking the elements of $X_{i,r,f}$ on top of each other for $i = 1, \ldots, 34$. We fit the FOS regression model using the *mgcv* package in *R* as follows:

```
model_rf = gam(y ~ s(t), data=X_rf);
```

The fit model_rf contains the fitted values indicating the mean effect of CGRP over time along with p-values for both the intercept and function-over-time components $\beta_{r,f}$ and $s_{r,f}(t)$

respectively. We plotted each model's fitted values along with a two-standard error region. When these two-standard error confidence regions contain zero, we interpret this as indicating no significant CGRP effect at that point in time.

Analysis of Sumatriptan over time

We computed the 30-second rolling means for the post-injection time series using the *tf_smooth* function from the R library *tf*[108] as described above.

For the power analysis, we computed 30-second rolling means over each mouse's log-power post-injection time series on the days they received the CGRP-only and CGRP-with-Sumatriptan injections. This was done for each frequency band and each brain region, resulting in two log-power 30-second rolling mean post-injection time series for each frequency band in a brain region, one for CGRP-only and the other for CGRP-with-Sumatriptan injections. Next, we computed the average and one standard deviation of the two time series across all mice. This gave us one mean CGRP-only log-power time series, one mean CGRP-with-Sumatriptan log-power time series, and their respective one standard deviation time series for each frequency band in each brain region. For each frequency band in each brain region, we plotted the CGRP-only and CGRP-with-Sumatriptan 30-second rolling mean time series together for comparison again using the *R* packages *ggplot2* [107] and *tidyfun*[108].

We processed the coherence data in the same manner. This resulted in one mean CGRP-only log-odds coherence 30-second rolling mean time series, one mean CGRP-with-Sumatriptan log-odds coherence 30-second rolling mean time series, and their respective one standard deviation time series for each

frequency band across each pair of brain regions. We plotted these 30-second rolling mean time series together for comparison, in the same way as we did for the log-power analyses.

The power and coherence FOS GAM analyses follow the previous section. For every mouse, we obtained a pairwise power difference time series for each frequency band in each brain region by subtracting each mouse's log-power CGRP-with-Sumatriptan time series from the corresponding CGRP-only time series. Similarly, for the coherence analysis, we obtained the pairwise difference time series for each frequency band across each pair of brain regions for each mouse by subtracting each mouse's log-odds coherence CGRP-with-Sumatriptan time series from the corresponding CGRP-only time series.
For the power and coherence analyses, we used a function-on-scalar regression using the *gam* function in the *R* package *mgcv*[109]. Each model had the same form as equation (1) above and was fit in the same manner as the previous experiment. We plotted the fitted values along with two-standard error confidence bands and obtained each model's p-values corresponding to the intercept and function-over-time components $\beta_{r,f}$ and $s_{r,f}(t)$ respectively.

Analysis of Early Life Stress Data over Time

We preprocessed the power and coherence data as described above. This experiment differed from the previous two experiments in that each treatment group consisted of different mice.

We computed the 30 second rolling mean plots in a similar manner as the previous two experiments using the *tf_smooth* function in the *R* library *tf* (Scheipl & Goldsmith, 2024). For the power analysis we first computed 30 second rolling means over each mouse's log-power post-injection time series on the days that they received CGRP injections so that each mouse had a CGRP log-power 30 second rolling mean post-injection time series for each frequency band for each brain region. We then computed the

average and one standard deviation CGRP log-power 30 second rolling mean time series across ELS mice along with the average and one standard deviation CGRP log power 30 second rolling mean time series across control mice so that we had one mean CGRP log-power time series for ELS, one mean CGRP log-power time series for control and their respective one standard deviation time series for each frequency band for each brain region. For each frequency band for each brain region, we plotted these 30 second rolling mean time series together for comparison in the same manner as the previous experiments.

We processed the coherence data in the same way so that we had one mean CGRP log-odds coherence 30 second rolling mean time series for ELS, one mean CGRP log-odds coherence 30 second rolling mean time series for control and their respective one standard deviation time series for each frequency band for each pair of brain regions. We plotted these 30 second rolling mean time series together for comparison in the same manner as the log-power analyses.

The different experimental design required us to use a different GAM model. For the power analysis, we performed FOS GAM analyses for each frequency band in each brain region with log power as the response and ELS or control as the covariates. Similarly, for the coherence analysis, we performed FOS GAM analyses for each frequency band in each pair of brain regions with log odds coherence as the response and ELS or control as the covariates. Each model had the following form:

$$y_{r,f}(t) = \beta_{r,f} + s_{r,f}(t) + els \cdot s'_{r,f}(t) + \varepsilon_{r,f}(t),$$

where $y_{r,f}(t)$ denotes the log-power or log-odds coherence at time point *t,* brain region (for power) or pair of regions (for coherence) *r* and frequency band *f*; $\beta_{r,f}$ denotes the *(r, f)*-specific model intercept; $s_{r,f}(t)$ denotes the *(r, f)*-specific model smooth function-over-time effect at time point t; *els* is a variable indicating whether the observation belongs to the ELS or control group; $s'_{r,f}(t)$ is the *(r, f)*-specific model smooth function-over-time effect due to the ELS treatment; and $\varepsilon_{r,f}(t)$ denotes *(r, f)*-specific

independent centered Gaussian noise at time point t. This FOS regression model assumes that the log-power or log-odds coherence are frequency band and region- or pair-specific functions of time.

We fit this model in *R* as follows. For the mouse *i*, $X_{i,r,f}$ denotes the *R* data.frame with columns representing time, ELS vs. control labels and response, where *t* is the vector of evenly spaced time steps, *els* is the vector of ones and zeros indicating whether an observation is associated with and ELS or control mouse and y denotes the observed log-power or log-odds coherence for mouse i in brain region or pair of brain regions *r* and frequency band *f*. Let *X_rf* denote the data.frame formed by stacking the elements of $X_{i,r,f}$ on top of each other for $i = 1, \ldots, 11$. We fit the FOS using the *mgcv* package in *R* as follows:

```
model_rf = gam(y ~ s(t) + s(t, by=els) , data=X_rf);
```

From the fit model_rf, we obtained the $s'_{r,f}(t)$ component of the fitted values which provides the estimated difference between the ELS and control effects over time in the same way that the previous models' estimates to $y_{r,f}(t)$ provide the estimated difference between treatment effects over time. We plotted these fitted values over time along with a two standard error confidence band, and we reported the p-values associated with each model's ELS-specific smooth function-over-time parameter $s'_{r,f}(t)$.

We took all of the p-values obtained from each experiment's analyses and computed FDR corrections on them in order to perform multiple comparisons hypothesis tests of whether or not there was a significant difference in treatment effects over time for a given brain region or pair of brain regions in a particular frequency band.

Changepoint analysis

Changepoint analysis was carried out as originally described in Zhang & Chan (2024) [110]. For this analysis, we evaluated the data in the two frequency bands we found to be most impacted by peripheral CGRP (4-7Hz and 8-13 Hz).

For conciseness, we shall simply describe the case of detecting changes in the 4-7 Hz component of the LFP, as the approach is the same for both frequency bands. Specifically, for each mouse, the 8-dimensional LFP times series are blocked into non-overlapping 10-second blocks, over each of which (i) we computed its smooth spectral density matrix estimate (as a function of frequency with 1 Hz steps) via a Bartlett window, (ii) normalized the spectral density matrix estimates so that their diagonal elements are identically equal to 1 and the off-diagonal elements measuring the LFP coherency between pairs of brain regions, and (iii) summarized the normalized spectral density matrix function by averaging over the 4-7 Hz.

The matrices per the 10-second blocks are 8 by 8 complex valued matrices, and their real part can be interpreted as proportional to the correlation matrix of the 8-dimensional 4-7 Hz (periodic) components of the LFP time series, with the latter denoted as Ξ_t for the t-th block (section 7.1 in Brillinger (2001)[111]. The change-point detection then proceeds to find the epochs (i.e. the change points, if they exist) across which Ξ_t's undergo a change, as follows. Let ν denote the projection vector, of unit length, pointing the principal direction of the change in Ξ_t, i.e., the quadratic form $\nu^{\top}\Xi_t\,\nu$ changes the most across the change point, among any unit directional vectors. The projection ν is then the principal direction along which the pre- and post-change-point correlation matrices of the 4-7 Hz periodic components of LFP differ from each other to the greatest extent.

The projection vectors reveal the structure of the change of the coherency matrix over the detected change point. Larger values in magnitude indicates larger changes for the corresponding brain regions.

Opposite signs within the projection vector are indicative of two major types of organizational matrix changes, which can be identified as blocks within the change in coherency matrix across the changepoint. These blocks can segregate coherency into activity within a subgroup of brain regions as two groups and activity between the subgroups (as in Fig. 7E). If the projection comprises coefficients of opposite signs, the brain regions are split into two groups according to the signs and may signify that across the change point, the inter-brain-region correlations between the two groups change differently, i.e., a variably heightened or lessened synchrony between the two groups, while there are no within-group changes. In the case that all coefficients of the projection vector are of the same sign, the correlations between brain regions of the 4-7 Hz periodic LFP components change in a more uniform way to an extent proportional to the product of their coefficients in the projection vector, i.e., a variably heightened or lessened synchrony across the 8 brain regions. The projection then comprises the direction of change in each brain region's LFPs along which the coherency structure of the LFPs sustains a change after induction by CGRP.

Clustering

For each possible combination pair of mice, we calculated the cosine distance between their projection directions. We then used this distance for k-medoids clustering. The number of clusters is estimated by optimum average silhouette width. And the clustering procedure is implemented on each of the three days for each frequency band.

Acknowledgements

We would like to thank our funding agencies who supported this work: 1DP2MH126377-01 (RH), the McKnight Foundation McKnight Neurobiology of Brain Disorders Award (RH), the Roy J. Carver Charitable Trust (RH), NINDS T32NS007124 (MJ, SM, and YF), Ramon D. Buckley Graduate Student

Award (MJ) and NSF Graduate Research Fellowship 1945994 (ME). We would also like to thank Andy Russo and Levi Sowers for helpful conversations and pharmacological expertise.

Declaration of Interests

The authors have nothing to declare.

References

1. Steiner, T.J., Stovner, L.J., Jensen, R., Uluduz, D., Katsarava, Z., and Lifting The Burden: the Global Campaign against, H. (2020). Migraine remains second among the world's causes of disability, and first among young women: findings from GBD2019. J Headache Pain *21*, 137. 10.1186/s10194-020-01208-0.
2. Headache Classification Committee of the International Headache Society (IHS) The International Classification of Headache Disorders, 3rd edition. (2018). Cephalalgia *38*, 1-211. 10.1177/0333102417738202.
3. Goadsby, P.J., Holland, P.R., Martins-Oliveira, M., Hoffmann, J., Schankin, C., and Akerman, S. (2017). Pathophysiology of Migraine: A Disorder of Sensory Processing. Physiol Rev *97*, 553-622. 10.1152/physrev.00034.2015.
4. Russo, A.F., and Hay, D.L. (2023). CGRP physiology, pharmacology, and therapeutic targets: migraine and beyond. Physiol Rev *103*, 1565-1644. 10.1152/physrev.00059.2021.
5. Schwedt, T.J., Chiang, C.C., Chong, C.D., and Dodick, D.W. (2015). Functional MRI of migraine. Lancet Neurol *14*, 81-91. 10.1016/S1474-4422(14)70193-0.
6. Schwedt, T.J. (2013). Multisensory integration in migraine. Curr Opin Neurol *26*, 248-253. 10.1097/WCO.0b013e328360edb1.
7. Schwedt, T.J., Schlaggar, B.L., Mar, S., Nolan, T., Coalson, R.S., Nardos, B., Benzinger, T., and Larson-Prior, L.J. (2013). Atypical resting-state functional connectivity of affective pain regions in chronic migraine. Headache *53*, 737-751. 10.1111/head.12081.
8. Schmidt, K., Schunke, O., Forkmann, K., and Bingel, U. (2015). Enhanced short-term sensitization of facial compared with limb heat pain. J Pain *16*, 781-790. 10.1016/j.jpain.2015.05.003.
9. Smith, J.G., Elias, L.A., Yilmaz, Z., Barker, S., Shah, K., Shah, S., and Renton, T. (2013). The psychosocial and affective burden of posttraumatic neuropathy following injuries to the trigeminal nerve. J Orofac Pain *27*, 293-303. 10.11607/jop.1056.
10. Schmidt, K., Forkmann, K., Sinke, C., Gratz, M., Bitz, A., and Bingel, U. (2016). The differential effect of trigeminal vs. peripheral pain stimulation on visual processing and memory encoding is influenced by pain-related fear. Neuroimage *134*, 386-395. 10.1016/j.neuroimage.2016.03.026.
11. Charles, A. (2018). The pathophysiology of migraine: implications for clinical management. Lancet Neurol *17*, 174-182. 10.1016/S1474-4422(17)30435-0.
12. Baliki, M.N., Chialvo, D.R., Geha, P.Y., Levy, R.M., Harden, R.N., Parrish, T.B., and Apkarian, A.V. (2006). Chronic pain and the emotional brain: specific brain activity associated with spontaneous fluctuations of intensity of chronic back pain. J Neurosci *26*, 12165-12173. 10.1523/JNEUROSCI.3576-06.2006.
13. Valfre, W., Rainero, I., Bergui, M., and Pinessi, L. (2008). Voxel-based morphometry reveals gray matter abnormalities in migraine. Headache *48*, 109-117. 10.1111/j.1526-4610.2007.00723.x.

14. Han, S., Soleiman, M.T., Soden, M.E., Zweifel, L.S., and Palmiter, R.D. (2015). Elucidating an Affective Pain Circuit that Creates a Threat Memory. Cell *162*, 363-374. 10.1016/j.cell.2015.05.057.
15. Corder, G., Ahanonu, B., Grewe, B.F., Wang, D., Schnitzer, M.J., and Scherrer, G. (2019). An amygdalar neural ensemble that encodes the unpleasantness of pain. Science *363*, 276-281. 10.1126/science.aap8586.
16. Chong, C.D., Gaw, N., Fu, Y., Li, J., Wu, T., and Schwedt, T.J. (2017). Migraine classification using magnetic resonance imaging resting-state functional connectivity data. Cephalalgia *37*, 828-844. 10.1177/0333102416652091.
17. Schulte, L.H., Menz, M.M., Haaker, J., and May, A. (2020). The migraineur's brain networks: Continuous resting state fMRI over 30 days. Cephalalgia *40*, 1614-1621. 10.1177/0333102420951465.
18. Noseda, R., Jakubowski, M., Kainz, V., Borsook, D., and Burstein, R. (2011). Cortical projections of functionally identified thalamic trigeminovascular neurons: implications for migraine headache and its associated symptoms. The Journal of neuroscience : the official journal of the Society for Neuroscience *31*, 14204-14217. 10.1523/JNEUROSCI.3285-11.2011.
19. Noseda, R., Kainz, V., Jakubowski, M., Gooley, J.J., Saper, C.B., Digre, K., and Burstein, R. (2010). A neural mechanism for exacerbation of headache by light. Nat Neurosci *13*, 239-245. 10.1038/nn.2475.
20. Wilcox, S.L., Veggeberg, R., Lemme, J., Hodkinson, D.J., Scrivani, S., Burstein, R., Becerra, L., and Borsook, D. (2016). Increased Functional Activation of Limbic Brain Regions during Negative Emotional Processing in Migraine. Frontiers in human neuroscience *10*, 366. 10.3389/fnhum.2016.00366.
21. Roy, D.S., Zhang, Y., Halassa, M.M., and Feng, G. (2022). Thalamic subnetworks as units of function. Nat Neurosci *25*, 140-153. 10.1038/s41593-021-00996-1.
22. Chen, Z., Xiao, L., Liu, H., Zhang, Q., Wang, Q., Lv, Y., Zhai, Y., Zhang, J., Dong, S., Wei, X., and Rong, L. (2022). Altered thalamo-cortical functional connectivity in patients with vestibular migraine: a resting-state fMRI study. Neuroradiology *64*, 119-127. 10.1007/s00234-021-02777-w.
23. Sowers, L.P., Wang, M., Rea, B.J., Taugher, R.J., Kuburas, A., Kim, Y., Wemmie, J.A., Walker, C.S., Hay, D.L., and Russo, A.F. (2020). Stimulation of Posterior Thalamic Nuclei Induces Photophobic Behavior in Mice. Headache *60*, 1961-1981. 10.1111/head.13917.
24. Palmiter, R.D. (2018). The Parabrachial Nucleus: CGRP Neurons Function as a General Alarm. Trends in neurosciences *41*, 280-293. 10.1016/j.tins.2018.03.007.
25. Vila-Pueyo, M., Hoffmann, J., Romero-Reyes, M., and Akerman, S. (2019). Brain structure and function related to headache: Brainstem structure and function in headache. Cephalalgia *39*, 1635-1660. 10.1177/0333102418784698.
26. Karsan, N., Bose, P.R., O'Daly, O., Zelaya, F.O., and Goadsby, P.J. (2020). Alterations in Functional Connectivity During Different Phases of the Triggered Migraine Attack. Headache *60*, 1244-1258. 10.1111/head.13865.
27. Jia, Z., Chen, X., Tang, W., Zhao, D., and Yu, S. (2019). Atypical functional connectivity between the anterior cingulate cortex and other brain regions in a rat model of recurrent headache. Mol Pain *15*, 1744806919842483. 10.1177/1744806919842483.
28. Rodriguez, E., Sakurai, K., Xu, J., Chen, Y., Toda, K., Zhao, S., Han, B.X., Ryu, D., Yin, H., Liedtke, W., and Wang, F. (2017). A craniofacial-specific monosynaptic circuit enables heightened affective pain. Nat Neurosci *20*, 1734-1743. 10.1038/s41593-017-0012-1.

29. Krout, K.E., and Loewy, A.D. (2000). Parabrachial nucleus projections to midline and intralaminar thalamic nuclei of the rat. J Comp Neurol *428*, 475-494. 10.1002/1096-9861(20001218)428:3<475::aid-cne6>3.0.co;2-9.
30. Brennan, K.C., and Pietrobon, D. (2018). A Systems Neuroscience Approach to Migraine. Neuron *97*, 1004-1021. 10.1016/j.neuron.2018.01.029.
31. Wattiez, A.S., Wang, M., and Russo, A.F. (2019). CGRP in Animal Models of Migraine. Handb Exp Pharmacol *255*, 85-107. 10.1007/164_2018_187.
32. Mason, B.N., Kaiser, E.A., Kuburas, A., Loomis, M.M., Latham, J.A., Garcia-Martinez, L.F., and Russo, A.F. (2017). Induction of Migraine-Like Photophobic Behavior in Mice by Both Peripheral and Central CGRP Mechanisms. The Journal of neuroscience : the official journal of the Society for Neuroscience *37*, 204-216. 10.1523/JNEUROSCI.2967-16.2016.
33. Hansen, J.M., Hauge, A.W., Olesen, J., and Ashina, M. (2010). Calcitonin gene-related peptide triggers migraine-like attacks in patients with migraine with aura. Cephalalgia *30*, 1179-1186. 10.1177/0333102410368444.
34. Asghar, M.S., Hansen, A.E., Kapijimpanga, T., van der Geest, R.J., van der Koning, P., Larsson, H.B., Olesen, J., and Ashina, M. (2010). Dilation by CGRP of middle meningeal artery and reversal by sumatriptan in normal volunteers. Neurology *75*, 1520-1526. 10.1212/WNL.0b013e3181f9626a.
35. Ashina, M., Bendtsen, L., Jensen, R., Schifter, S., and Olesen, J. (2000). Evidence for increased plasma levels of calcitonin gene-related peptide in migraine outside of attacks. Pain *86*, 133-138. 10.1016/s0304-3959(00)00232-3.
36. Cernuda-Morollon, E., Larrosa, D., Ramon, C., Vega, J., Martinez-Camblor, P., and Pascual, J. (2013). Interictal increase of CGRP levels in peripheral blood as a biomarker for chronic migraine. Neurology *81*, 1191-1196. 10.1212/WNL.0b013e3182a6cb72.
37. Goadsby, P.J., Edvinsson, L., and Ekman, R. (1990). Vasoactive peptide release in the extracerebral circulation of humans during migraine headache. Ann Neurol *28*, 183-187. 10.1002/ana.410280213.
38. Edvinsson, L., Haanes, K.A., Warfvinge, K., and Krause, D.N. (2018). CGRP as the target of new migraine therapies - successful translation from bench to clinic. Nat Rev Neurol *14*, 338-350. 10.1038/s41582-018-0003-1.
39. Hultman, R., Mague, S.D., Li, Q., Katz, B.M., Michel, N., Lin, L., Wang, J., David, L.K., Blount, Chandy, R., Carlson, D., Ulrich, K., Carin, L., Dunson, Kumar, S., Deisseroth, K. Moore, S.D., Dzirasa, K. (2016). Prefrontal Cortex-Mediated Slow-Evolving Limbic Dynamics Drives Stress-Induced Emotional Pathology. Neuron *In Press*.
40. Kumar, S., Hultman, R., Hughes, D., Michel, N., Katz, B.M., and Dzirasa, K. (2014). Prefrontal cortex reactivity underlies trait vulnerability to chronic social defeat stress. Nature communications *5*, 4537. 10.1038/ncomms5537.
41. Adhikari, A., Topiwala, M.A., and Gordon, J.A. (2010). Synchronized activity between the ventral hippocampus and the medial prefrontal cortex during anxiety. Neuron *65*, 257-269. 10.1016/j.neuron.2009.12.002.
42. Hultman, R., Ulrich, K., Sachs, B.D., Blount, C., Carlson, D.E., Ndubuizu, N., Bagot, R.C., Parise, E.M., Vu, M.T., Gallagher, N.M., et al. (2018). Brain-wide Electrical Spatiotemporal Dynamics Encode Depression Vulnerability. Cell *173*, 166-180 e114. 10.1016/j.cell.2018.02.012.
43. Hultman, R., Mague, S.D., Li, Q., Katz, B.M., Michel, N., Lin, L., Wang, J., David, L.K., Blount, C., Chandy, R., et al. (2016). Dysregulation of Prefrontal Cortex-Mediated Slow-Evolving Limbic Dynamics Drives Stress-Induced Emotional Pathology. Neuron *91*, 439-452. 10.1016/j.neuron.2016.05.038.

44. Perge, J.A., Zhang, S., Malik, W.Q., Homer, M.L., Cash, S., Friehs, G., Eskandar, E.N., Donoghue, J.P., and Hochberg, L.R. (2014). Reliability of directional information in unsorted spikes and local field potentials recorded in human motor cortex. J Neural Eng *11*, 046007. 10.1088/1741-2560/11/4/046007.
45. Schaich Borg, J., Srivastava, S., Lin, L., Heffner, J., Dunson, D., Dzirasa, K., and de Lecea, L. (2017). Rat intersubjective decisions are encoded by frequency-specific oscillatory contexts. Brain Behav *7*, e00710. 10.1002/brb3.710.
46. Nolte, G., Ziehe, A., Nikulin, V.V., Schlogl, A., Kramer, N., Brismar, T., and Muller, K.R. (2008). Robustly estimating the flow direction of information in complex physical systems. Phys Rev Lett *100*, 234101. 10.1103/PhysRevLett.100.234101.
47. Dzirasa, K., Fuentes, R., Kumar, S., Potes, J.M., and Nicolelis, M.A. (2011). Chronic in vivo multi-circuit neurophysiological recordings in mice. Journal of neuroscience methods *195*, 36-46. 10.1016/j.jneumeth.2010.11.014.
48. Adhikari, A., Sigurdsson, T., Topiwala, M.A., and Gordon, J.A. (2010). Cross-correlation of instantaneous amplitudes of field potential oscillations: a straightforward method to estimate the directionality and lag between brain areas. J Neurosci Methods *191*, 191-200. 10.1016/j.jneumeth.2010.06.019.
49. Buzsàki, G., and Eidelberg, E. (1983). Phase relations of hippocampal projection cells and interneurons to theta activity in the anesthetized rat. Brain research *266*, 334-339. 10.1016/0006-8993(83)90665-0.
50. GREEN, J.D., and ARDUINI, A.A. (1954). Hippocampal electrical activity in arousal. J Neurophysiol *17*, 533-557. 10.1152/jn.1954.17.6.533.
51. Gordon, J.A., Lacefield, C.O., Kentros, C.G., and Hen, R. (2005). State-dependent alterations in hippocampal oscillations in serotonin 1A receptor-deficient mice. The Journal of neuroscience : the official journal of the Society for Neuroscience *25*, 6509-6519. 10.1523/jneurosci.1211-05.2005.
52. Winson, J., and Abzug, C. (1978). Neuronal transmission through hippocampal pathways dependent on behavior. J Neurophysiol *41*, 716-732. 10.1152/jn.1978.41.3.716.
53. Padilla-Coreano, N., Canetta, S., Mikofsky, R.M., Alway, E., Passecker, J., Myroshnychenko, M.V., Garcia-Garcia, A.L., Warren, R., Teboul, E., Blackman, D.R., et al. (2019). Hippocampal-Prefrontal Theta Transmission Regulates Avoidance Behavior. Neuron *104*, 601-610.e604. 10.1016/j.neuron.2019.08.006.
54. Adhikari, A., Topiwala, M.A., and Gordon, J.A. (2010). Synchronized Activity between the Ventral Hippocampus and the Medial Prefrontal Cortex during Anxiety. Neuron *65*, 257-269.
55. Rea, B.J., Wattiez, A.S., Waite, J.S., Castonguay, W.C., Schmidt, C.M., Fairbanks, A.M., Robertson, B.R., Brown, C.J., Mason, B.N., Moldovan-Loomis, M.C., et al. (2018). Peripherally Administered CGRP Induces Spontaneous Pain in Mice: Implications for Migraine. Pain. 10.1097/j.pain.0000000000001337.
56. Valentinova, K., Acuna, M.A., Ntamati, N.R., Nevian, N.E., and Nevian, T. (2023). An amygdala-to-cingulate cortex circuit for conflicting choices in chronic pain. Cell Rep *42*, 113125. 10.1016/j.celrep.2023.113125.
57. Veinante, P., Yalcin, I., and Barrot, M. (2013). The amygdala between sensation and affect: a role in pain. J Mol Psychiatry *1*, 9. 10.1186/2049-9256-1-9.
58. Cameron, C., Kelly, S., Hsieh, S.C., Murphy, M., Chen, L., Kotb, A., Peterson, J., Coyle, D., Skidmore, B., Gomes, T., et al. (2015). Triptans in the Acute Treatment of Migraine: A Systematic Review and Network Meta-Analysis. Headache *55 Suppl 4*, 221-235. 10.1111/head.12601.

59. Holland, P.R., Sureda-Gibert, P., and Vila-Pueyo, M. (2020). Rapid uptake of sumatriptan into the brain: An ongoing question of blood-brain barrier permeability. Cephalalgia *40*, 327-329. 10.1177/0333102420905131.
60. Tfelt-Hansen, P.C. (2010). Does sumatriptan cross the blood-brain barrier in animals and man? J Headache Pain *11*, 5-12. 10.1007/s10194-009-0170-y.
61. Becerra, L., Bishop, J., Barmettler, G., Xie, Y., Navratilova, E., Porreca, F., and Borsook, D. (2016). Triptans disrupt brain networks and promote stress-induced CSD-like responses in cortical and subcortical areas. J Neurophysiol *115*, 208-217. 10.1152/jn.00632.2015.
62. Anda, R.F., Felitti, V.J., Bremner, J.D., Walker, J.D., Whitfield, C., Perry, B.D., Dube, S.R., and Giles, W.H. (2006). The enduring effects of abuse and related adverse experiences in childhood. A convergence of evidence from neurobiology and epidemiology. Eur Arch Psychiatry Clin Neurosci *256*, 174-186. 10.1007/s00406-005-0624-4.
63. Zhai, Z.W., Yip, S.W., Lacadie, C.M., Sinha, R., Mayes, L.C., and Potenza, M.N. (2019). Childhood trauma moderates inhibitory control and anterior cingulate cortex activation during stress. Neuroimage *185*, 111-118. 10.1016/j.neuroimage.2018.10.049.
64. Jaramillo, A.A., Brown, J.A., and Winder, D.G. (2021). Danger and distress: Parabrachial-extended amygdala circuits. Neuropharmacology *198*, 108757. 10.1016/j.neuropharm.2021.108757.
65. Holschneider, D.P., Guo, Y., Mayer, E.A., and Wang, Z. (2016). Early life stress elicits visceral hyperalgesia and functional reorganization of pain circuits in adult rats. Neurobiol Stress *3*, 8-22. 10.1016/j.ynstr.2015.12.003.
66. Fuller-Thomson, E., Baker, T.M., and Brennenstuhl, S. (2010). Investigating the association between childhood physical abuse and migraine. Headache *50*, 749-760. 10.1111/j.1526-4610.2010.01626.x.
67. Anda, R., Tietjen, G., Schulman, E., Felitti, V., and Croft, J. (2010). Adverse childhood experiences and frequent headaches in adults. Headache *50*, 1473-1481. 10.1111/j.1526-4610.2010.01756.x.
68. Raoof, M., Amanpour, S., Roghani, A., Abbasnejad, M., Kooshki, R., Askari-Zahabi, K., Mohamadi-Jorjafki, E., Majdzadeh, B., Aarab, G., and Lobbezoo, F. (2022). The effects of neonatal maternal deprivation and chronic unpredictable stresses on migraine-like behaviors in adult rats. Neurosci Lett *772*, 136444. 10.1016/j.neulet.2022.136444.
69. Eller, O.C., Yang, X., Fuentes, I.M., Pierce, A.N., Jones, B.M., Brake, A.D., Wang, R., Dussor, G., and Christianson, J.A. (2021). Voluntary Wheel Running Partially Attenuates Early Life Stress-Induced Neuroimmune Measures in the Dura and Evoked Migraine-Like Behaviors in Female Mice. Front Physiol *12*, 665732. 10.3389/fphys.2021.665732.
70. Minguez-Olaondo, A., Quintas, S., Morollon Sanchez-Mateos, N., Lopez-Bravo, A., Vila-Pueyo, M., Grozeva, V., Belvis, R., Santos-Lasaosa, S., and Irimia, P. (2021). Cutaneous Allodynia in Migraine: A Narrative Review. Front Neurol *12*, 831035. 10.3389/fneur.2021.831035.
71. Munjal, S., Singh, P., Reed, M.L., Fanning, K., Schwedt, T.J., Dodick, D.W., Buse, D.C., and Lipton, R.B. (2020). Most Bothersome Symptom in Persons With Migraine: Results From the Migraine in America Symptoms and Treatment (MAST) Study. Headache *60*, 416-429. 10.1111/head.13708.
72. Wang, M., Mason, B.N., Sowers, L.P., Kuburas, A., Rea, B.J., and Russo, A.F. (2021). Investigating Migraine-Like Behavior Using Light Aversion in Mice. J Vis Exp. 10.3791/62839.
73. Iyengar, S., Johnson, K.W., Ossipov, M.H., and Aurora, S.K. (2019). CGRP and the Trigeminal System in Migraine. Headache *59*, 659-681. 10.1111/head.13529.
74. Marciszewski, K.K., Meylakh, N., Di Pietro, F., Mills, E.P., Macefield, V.G., Macey, P.M., and Henderson, L.A. (2018). Changes in Brainstem Pain Modulation Circuitry Function over the Migraine Cycle. The Journal of neuroscience : the official journal of the Society for Neuroscience *38*, 10479-10488. 10.1523/JNEUROSCI.1088-18.2018.

75. Messina, R., Gollion, C., Christensen, R.H., and Amin, F.M. (2022). Functional MRI in migraine. Curr Opin Neurol *35*, 328-335. 10.1097/WCO.0000000000001060.
76. Deen, M., Correnti, E., Kamm, K., Kelderman, T., Papetti, L., Rubio-Beltran, E., Vigneri, S., Edvinsson, L., Maassen Van Den Brink, A., and European Headache Federation School of Advanced, S. (2017). Blocking CGRP in migraine patients - a review of pros and cons. J Headache Pain *18*, 96. 10.1186/s10194-017-0807-1.
77. Ferrari, M.D., Goadsby, P.J., Burstein, R., Kurth, T., Ayata, C., Charles, A., Ashina, M., van den Maagdenberg, A., and Dodick, D.W. (2022). Migraine. Nat Rev Dis Primers *8*, 2. 10.1038/s41572-021-00328-4.
78. Mohanty, D., and Lippmann, S. (2020). CGRP Inhibitors for Migraine. Innov Clin Neurosci *17*, 39-40.
79. Peters, G.L. (2019). Migraine overview and summary of current and emerging treatment options. Am J Manag Care *25*, S23-S34.
80. Hammond, N.G., and Colman, I. (2020). The Role of Positive Health Behaviors in the Relationship Between Early Life Stress and Migraine. Headache *60*, 1111-1123. 10.1111/head.13808.
81. Uddin, O., Anderson, M., Smith, J., Masri, R., and Keller, A. (2021). Parabrachial complex processes dura inputs through a direct trigeminal ganglion-to-parabrachial connection. Neurobiol Pain *9*, 100060. 10.1016/j.ynpai.2021.100060.
82. Han, J.S., Li, W., and Neugebauer, V. (2005). Critical role of calcitonin gene-related peptide 1 receptors in the amygdala in synaptic plasticity and pain behavior. The Journal of neuroscience : the official journal of the Society for Neuroscience *25*, 10717-10728. 10.1523/JNEUROSCI.4112-05.2005.
83. Eftekhari, S., Salvatore, C.A., Calamari, A., Kane, S.A., Tajti, J., and Edvinsson, L. (2010). Differential distribution of calcitonin gene-related peptide and its receptor components in the human trigeminal ganglion. Neuroscience *169*, 683-696. 10.1016/j.neuroscience.2010.05.016.
84. Guo, S., Vollesen, A.L.H., Olesen, J., and Ashina, M. (2016). Premonitory and nonheadache symptoms induced by CGRP and PACAP38 in patients with migraine. Pain *157*, 2773-2781. 10.1097/j.pain.0000000000000702.
85. Russo, A.F. (2015). Calcitonin gene-related peptide (CGRP): a new target for migraine. Annu Rev Pharmacol Toxicol *55*, 533-552. 10.1146/annurev-pharmtox-010814-124701.
86. Brar, Y., Hosseini, S.A., and Saadabadi, A. (2024). Sumatriptan. In StatPearls.
87. Durham, P.L., and Russo, A.F. (1999). Regulation of calcitonin gene-related peptide secretion by a serotonergic antimigraine drug. The Journal of neuroscience : the official journal of the Society for Neuroscience *19*, 3423-3429. 10.1523/JNEUROSCI.19-09-03423.1999.
88. Benemei, S., Cortese, F., Labastida-Ramirez, A., Marchese, F., Pellesi, L., Romoli, M., Vollesen, A.L., Lampl, C., Ashina, M., and School of Advanced Studies of the European Headache, F. (2017). Triptans and CGRP blockade - impact on the cranial vasculature. J Headache Pain *18*, 103. 10.1186/s10194-017-0811-5.
89. Asghar, M.S., Becerra, L., Larsson, H.B., Borsook, D., and Ashina, M. (2016). Calcitonin Gene-Related Peptide Modulates Heat Nociception in the Human Brain - An fMRI Study in Healthy Volunteers. PloS one *11*, e0150334. 10.1371/journal.pone.0150334.
90. Buse, D.C., Reed, M.L., Fanning, K.M., Bostic, R., Dodick, D.W., Schwedt, T.J., Munjal, S., Singh, P., and Lipton, R.B. (2020). Comorbid and co-occurring conditions in migraine and associated risk of increasing headache pain intensity and headache frequency: results of the migraine in America symptoms and treatment (MAST) study. J Headache Pain *21*, 23. 10.1186/s10194-020-1084-y.
91. Maleki, N., Becerra, L., and Borsook, D. (2012). Migraine: maladaptive brain responses to stress. Headache *52 Suppl 2*, 102-106. 10.1111/j.1526-4610.2012.02241.x.

92. Avona, A., Mason, B.N., Lackovic, J., Wajahat, N., Motina, M., Quigley, L., Burgos-Vega, C., Moldovan Loomis, C., Garcia-Martinez, L.F., Akopian, A.N., et al. (2020). Repetitive stress in mice causes migraine-like behaviors and calcitonin gene-related peptide-dependent hyperalgesic priming to a migraine trigger. Pain *161*, 2539-2550. 10.1097/j.pain.0000000000001953.
93. Allais, G., Chiarle, G., Sinigaglia, S., Airola, G., Schiapparelli, P., and Benedetto, C. (2020). Gender-related differences in migraine. Neurol Sci *41*, 429-436. 10.1007/s10072-020-04643-8.
94. White, J.D., Arefin, T.M., Pugliese, A., Lee, C.H., Gassen, J., Zhang, J., and Kaffman, A. (2020). Early life stress causes sex-specific changes in adult fronto-limbic connectivity that differentially drive learning. Elife *9*. 10.7554/eLife.58301.
95. Gracia-Rubio, I., Moscoso-Castro, M., Pozo, O.J., Marcos, J., Nadal, R., and Valverde, O. (2016). Maternal separation induces neuroinflammation and long-lasting emotional alterations in mice. Prog Neuropsychopharmacol Biol Psychiatry *65*, 104-117. 10.1016/j.pnpbp.2015.09.003.
96. Pena, C.J., Smith, M., Ramakrishnan, A., Cates, H.M., Bagot, R.C., Kronman, H.G., Patel, B., Chang, A.B., Purushothaman, I., Dudley, J., et al. (2019). Early life stress alters transcriptomic patterning across reward circuitry in male and female mice. Nature communications *10*, 5098. 10.1038/s41467-019-13085-6.
97. Kikusui, T., Isaka, Y., and Mori, Y. (2005). Early weaning deprives mouse pups of maternal care and decreases their maternal behavior in adulthood. Behav Brain Res *162*, 200-206. 10.1016/j.bbr.2005.03.013.
98. Chaplan, S.R., Bach, F.W., Pogrel, J.W., Chung, J.M., and Yaksh, T.L. (1994). Quantitative assessment of tactile allodynia in the rat paw. J Neurosci Methods *53*, 55-63. 10.1016/0165-0270(94)90144-9.
99. Dixon, W.J. (1980). Efficient analysis of experimental observations. Annu Rev Pharmacol Toxicol *20*, 441-462. 10.1146/annurev.pa.20.040180.002301.
100. Bates, D., Maechler, M., Bolker, B., Walker, S. (2015). Fitting Linear Mixed-Effects Models Using lme4. Journal of Statistical Software *67*, 1-48. doi:10.18637/jss.v067.i01.
101. Kuznetsova, A., Brockhoff, P.B., Christensen, R.H.B. (2017). lmerTest Package: Tests in Linear Mixed Effects Models. Journal of Statistical Software *82*, 1-26. doi: 10.18637/jss.v082.i13.
102. Tibshirani, R. (1996). Regression Shrinkage and Selection via the Lasso. J R Stat Soc Ser B. *58*, 267–288.
103. Tibshirani R, S.M., Rosset S, Zhu J, Knight K. (2005). Sparsity and smoothness via the fused lasso. J R Stat Soc Ser B (Statistical Methodol.) *67*, 91–108. doi:https://doi.org/10.1111/j.1467-9868.2005.00490.
104. Tibshirani RJ, T.J. (2011). THE SOLUTION PATH OF THE GENERALIZED LASSO. Ann Stat. *39*, 1335–1371.
105. Hastie, T., & Tibshirani, R. (1986). Generalized Additive Models. Statistical Science *1*, 297–310.
106. Scheipl, F.a.J.G., J. (2024). tf: S3 Classes and Methods for Tidy Functional Data.
107. Wickham, H. (2016). ggplot2: Elegant Graphics for Data Analysis. (Springer-Verlag).
108. Scheipl, F., Goldsmith, J. and Wrobel, J. (2024). tidyfun: Tools for Tidy Functional Data. https://github.com/tidyfun/tidyfun.
109. Wood, S.N. (2010). Fast Stable Restricted Maximum Likelihood and Marginal Likelihood Estimation of Semiparametric Generalized Linear Models. Journal of the Royal Statistical Society Series B: Statistical Methodology *73*, 3-36. 10.1111/j.1467-9868.2010.00749.x.
110. Zhang, X., Chan, K. (2024). Spectral Change Point Estimation for High Dimensional Time Series by Sparse Tensor Decomposition. In U.o. Iowa, ed. arxiv.
111. Brillinger, D.R. (2001). Time Series: Data Analysis and Theory (Society for Industrial and Applied Mathematics).

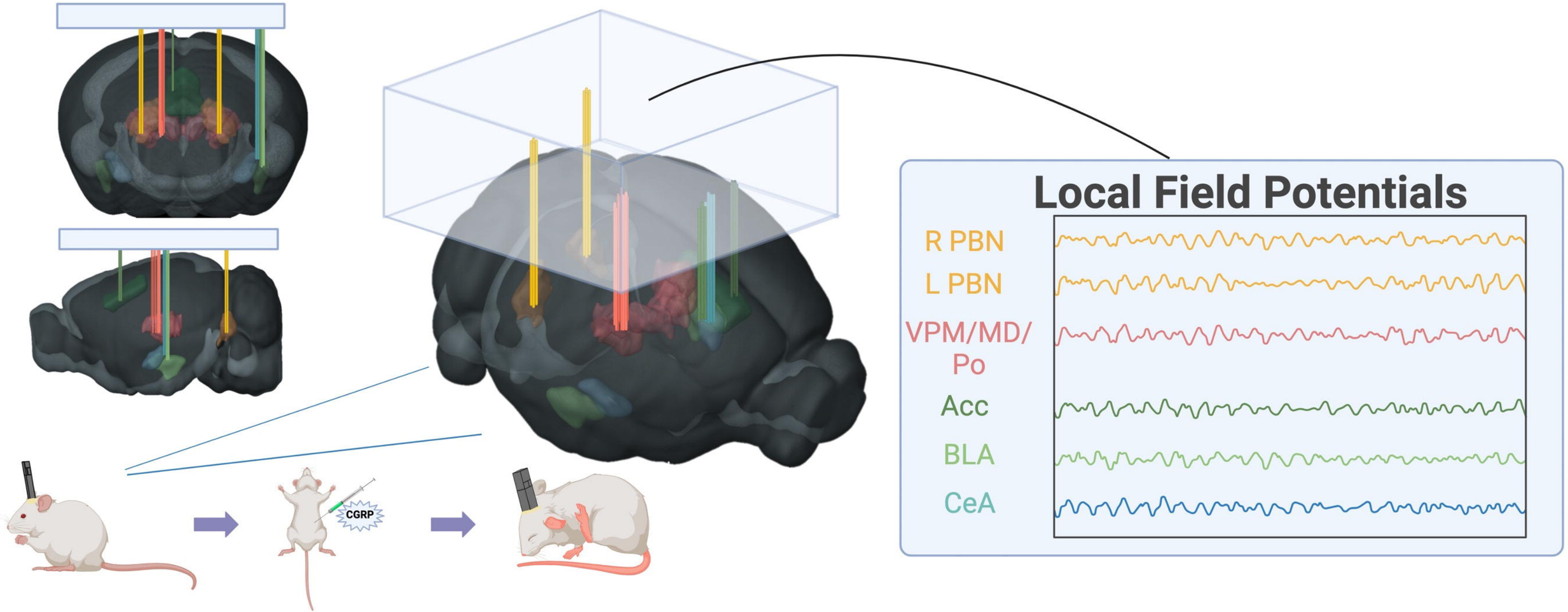
Local Field Potentials
R PBN
L PBN
VPM/MD/
Po
Acc
BLA
CeA
CGRP

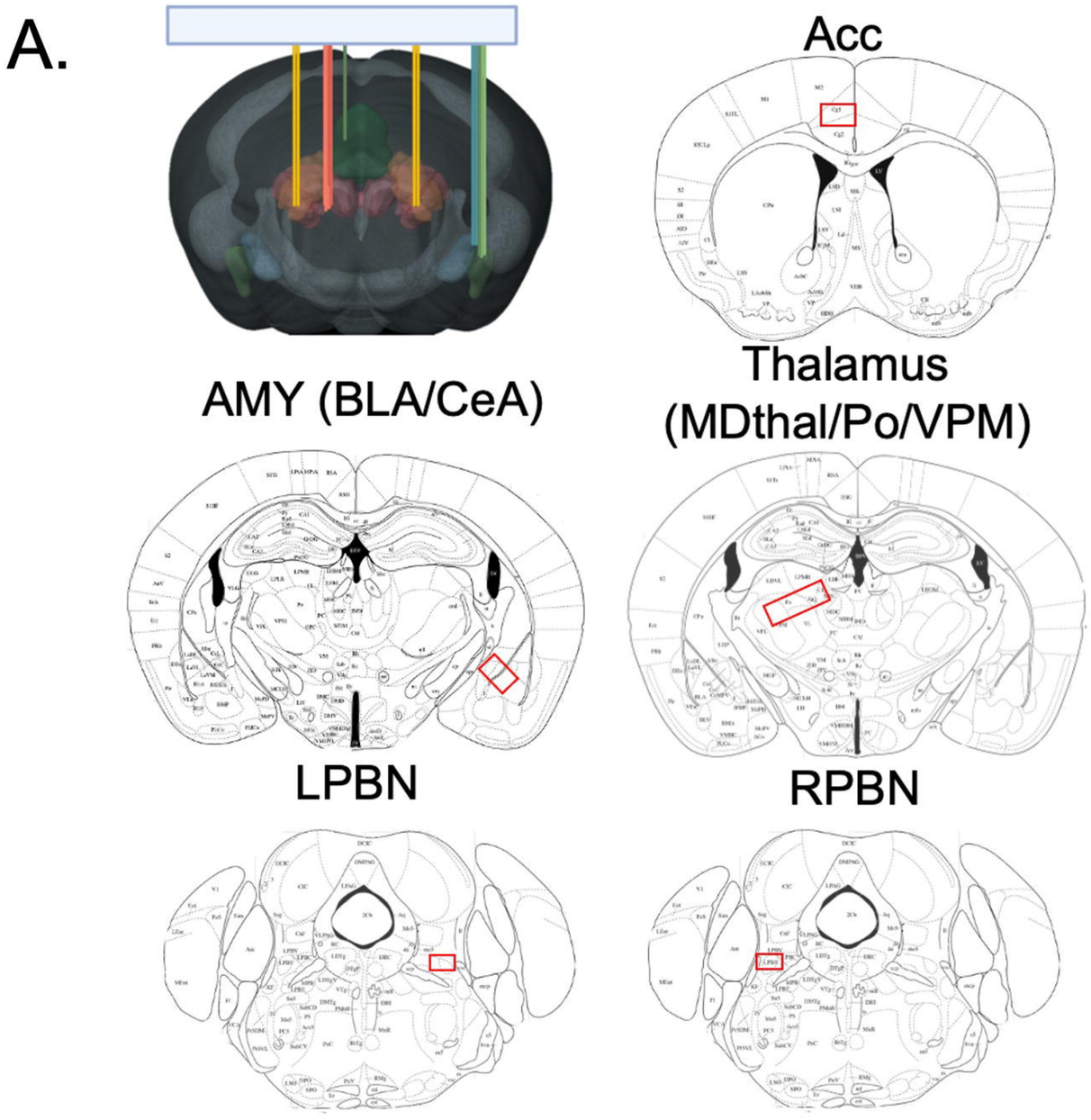
A.
Acc
AMY (BLA/CeA)
Thalamus
(MDthal/Po/VPM)
LPBN
RPBN

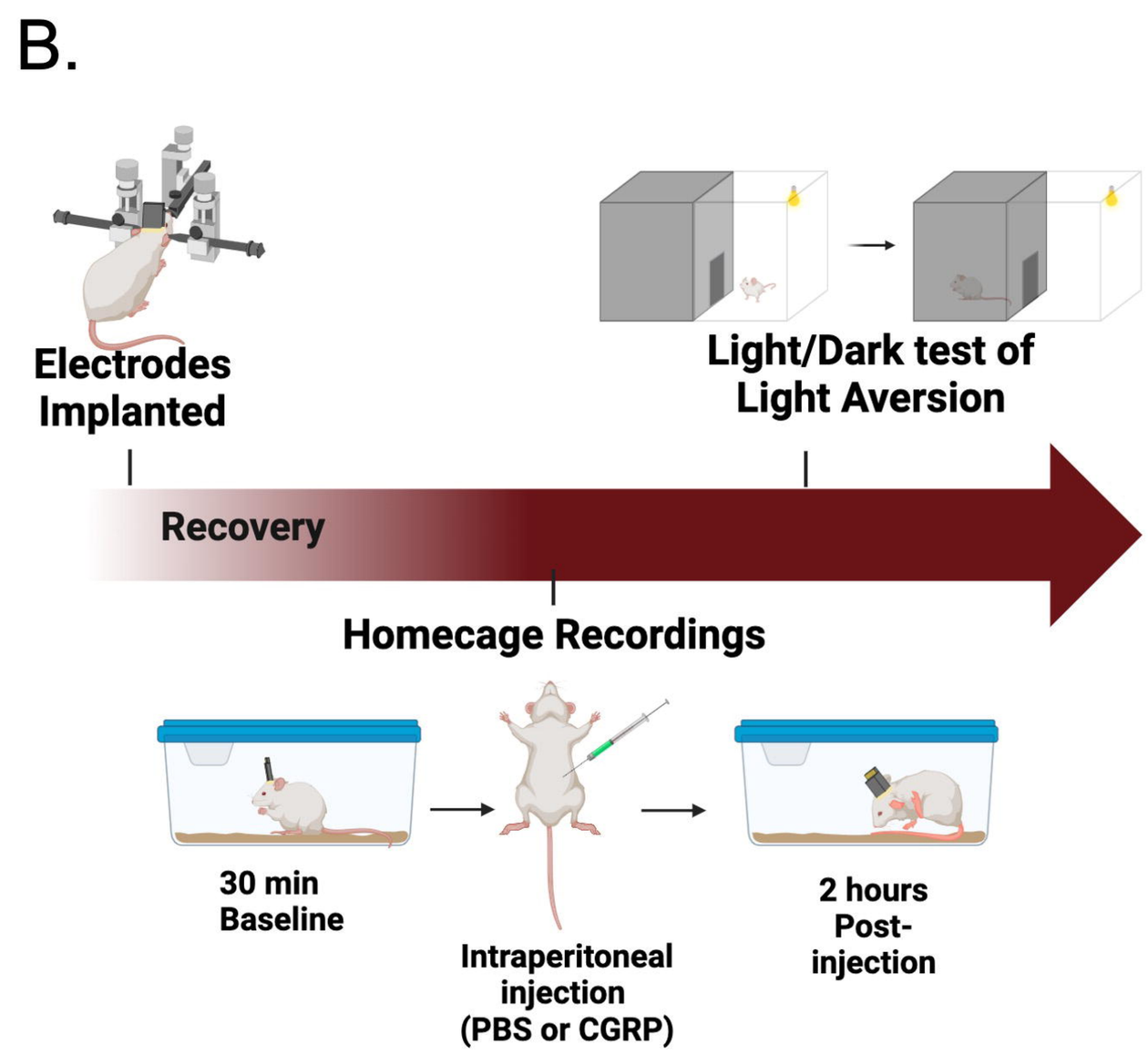
B.
Electrodes
Implanted
Light/Dark test of
Light Aversion
Recovery
Homecage Recordings
30 min
Baseline
Intraperitoneal
injection
(PBS or CGRP)
2 hours
Post-
injection

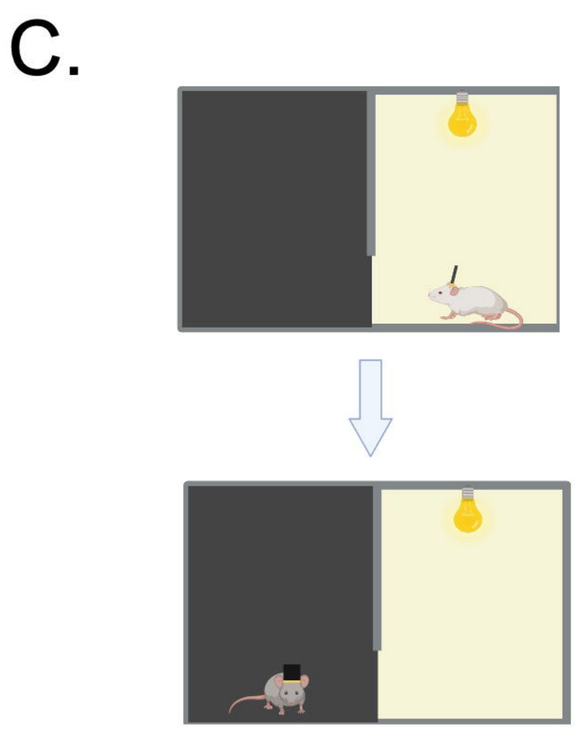
C.

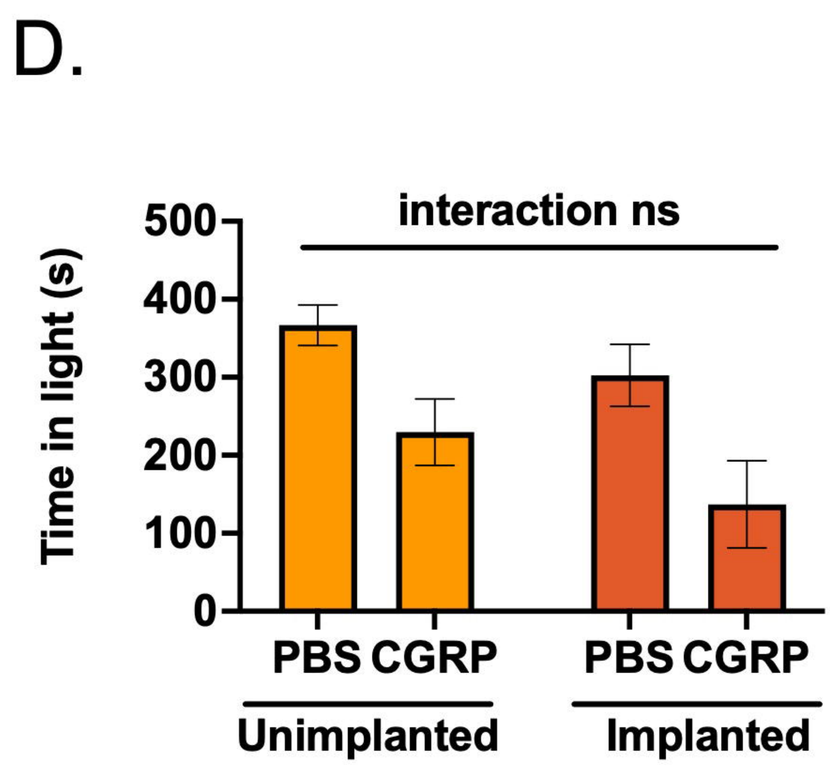
D.
interaction ns
Time in light (s)
500
400
300
200
100
0
PBS CGRP
PBS CGRP
Unimplanted
Implanted

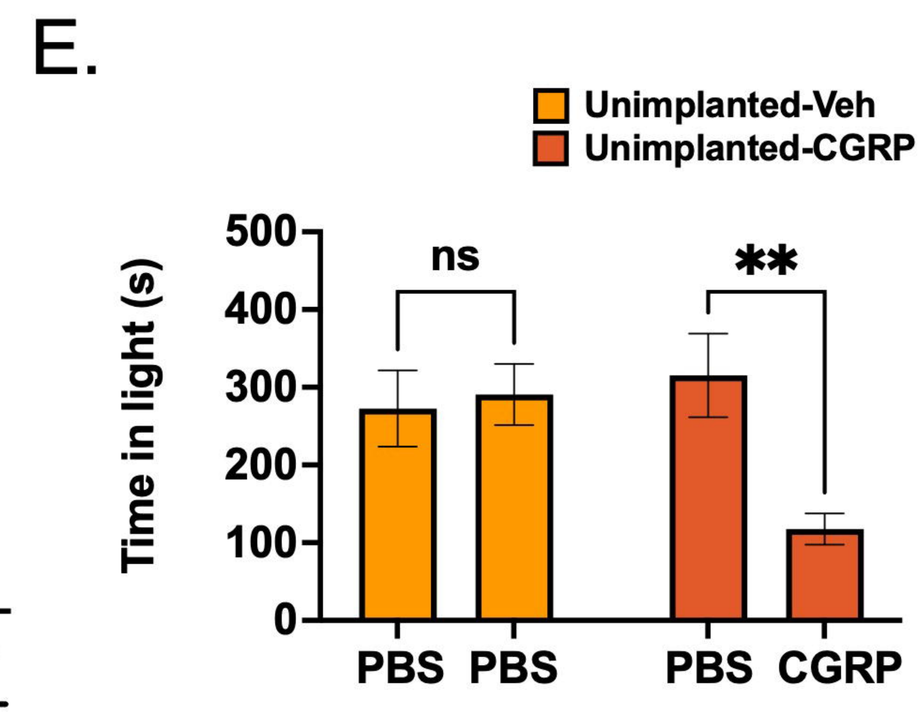
E.
Unimplanted-Veh
Unimplanted-CGRP
Time in light (s)
500
400
300
200
100
0
ns
**
PBS PBS
PBS CGRP

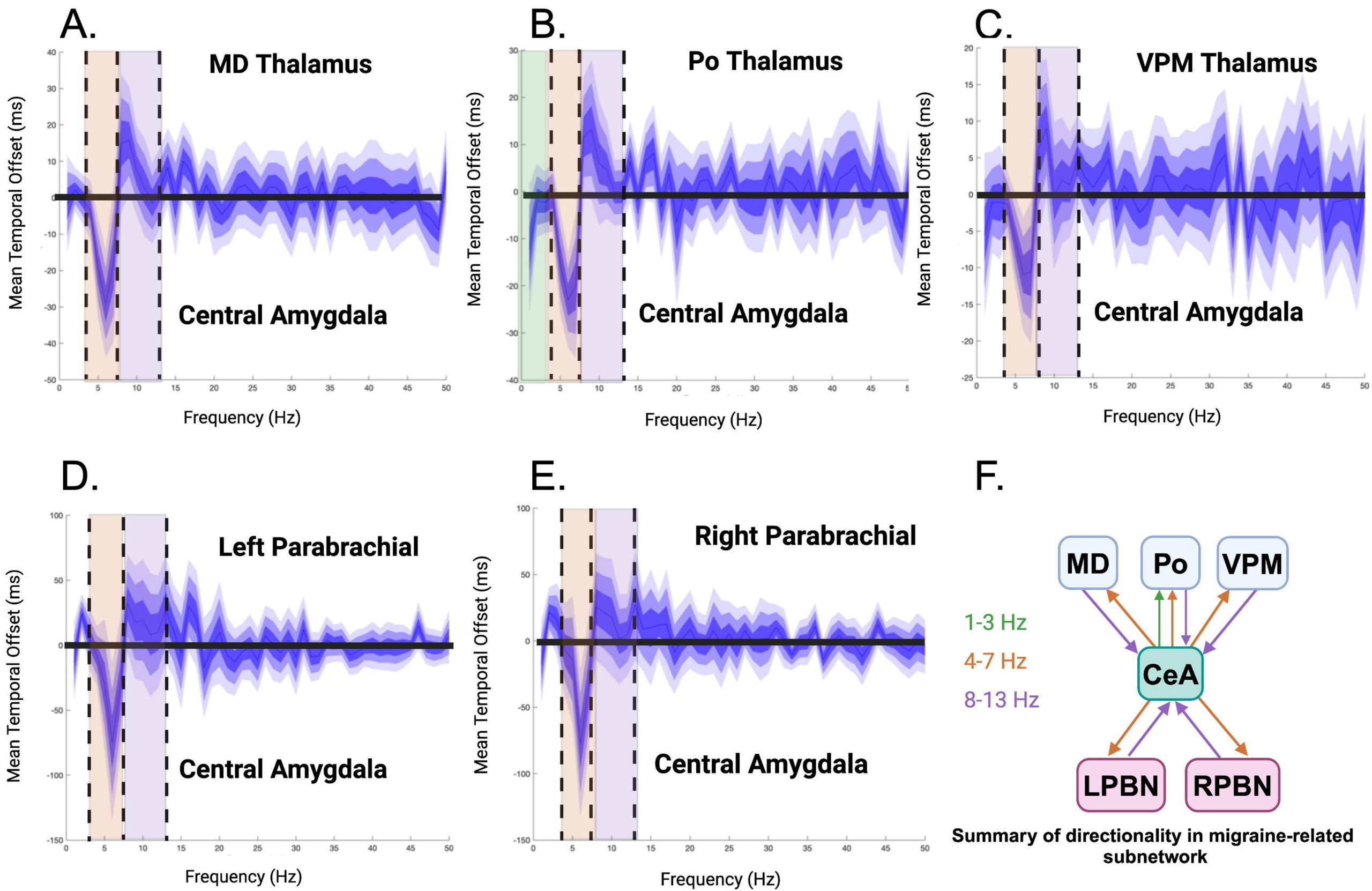
A.
MD Thalamus
Central Amygdala
Mean Temporal Offset (ms)
Frequency (Hz)
B.
Po Thalamus
Central Amygdala
Mean Temporal Offset (ms)
Frequency (Hz)
C.
VPM Thalamus
Central Amygdala
Mean Temporal Offset (ms)
Frequency (Hz)
D.
Left Parabrachial
Central Amygdala
Mean Temporal Offset (ms)
Frequency (Hz)
E.
Right Parabrachial
Central Amygdala
Mean Temporal Offset (ms)
Frequency (Hz)
F.
MD
Po
VPM
CeA
LPBN
RPBN
1-3 Hz
4-7 Hz
8-13 Hz
Summary of directionality in migraine-related subnetwork

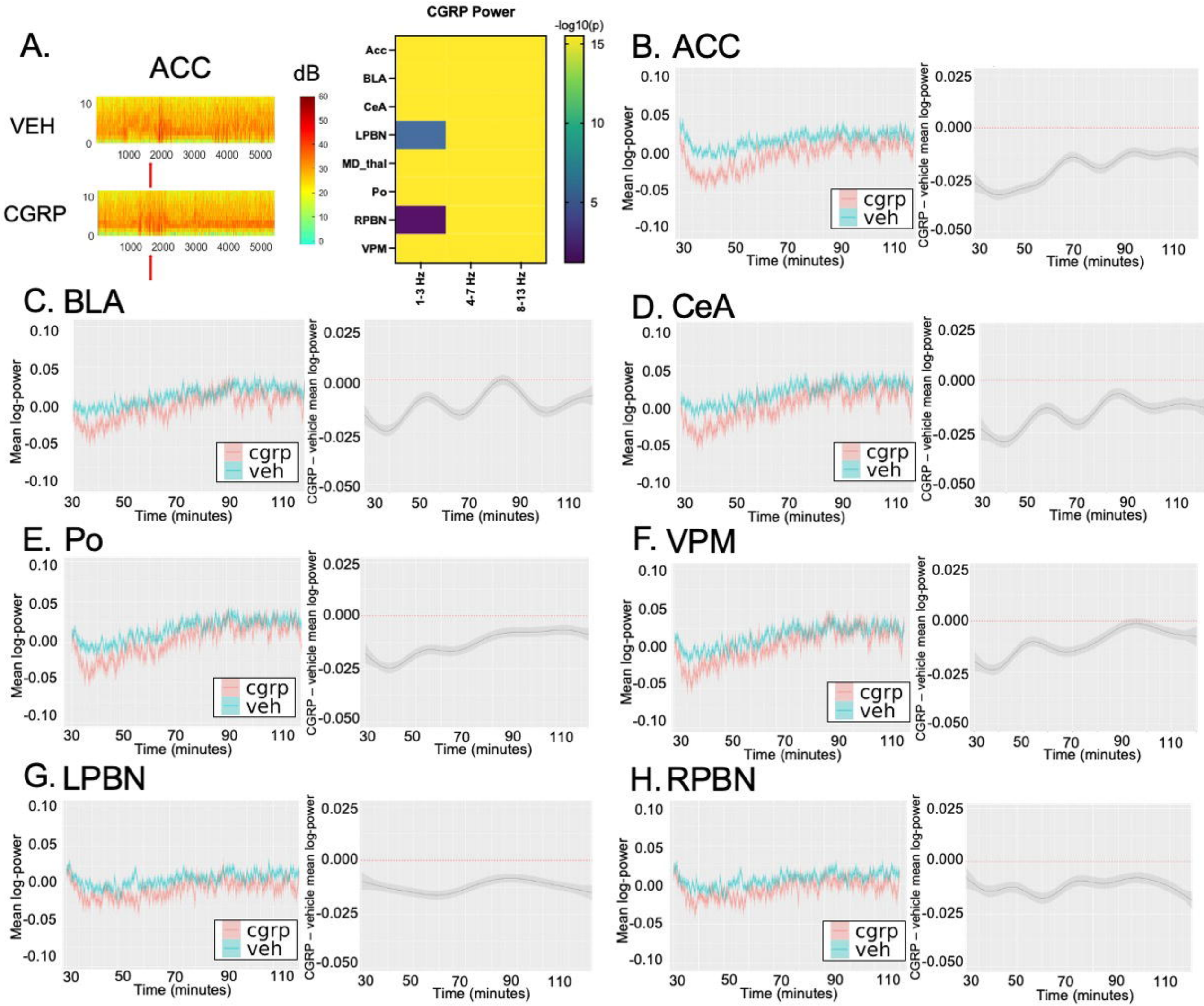
A.
ACC
VEH
CGRP
dB
CGRP Power
-log10(p)
Acc
BLA
CeA
LPBN
MD_thal
Po
RPBN
VPM
1-3 Hz
4-7 Hz
8-13 Hz
B. ACC
C. BLA
D. CeA
E. Po
F. VPM
G. LPBN
H. RPBN
Mean log-power
CGRP – vehicle mean log-power
Time (minutes)
cgrp
veh

A.

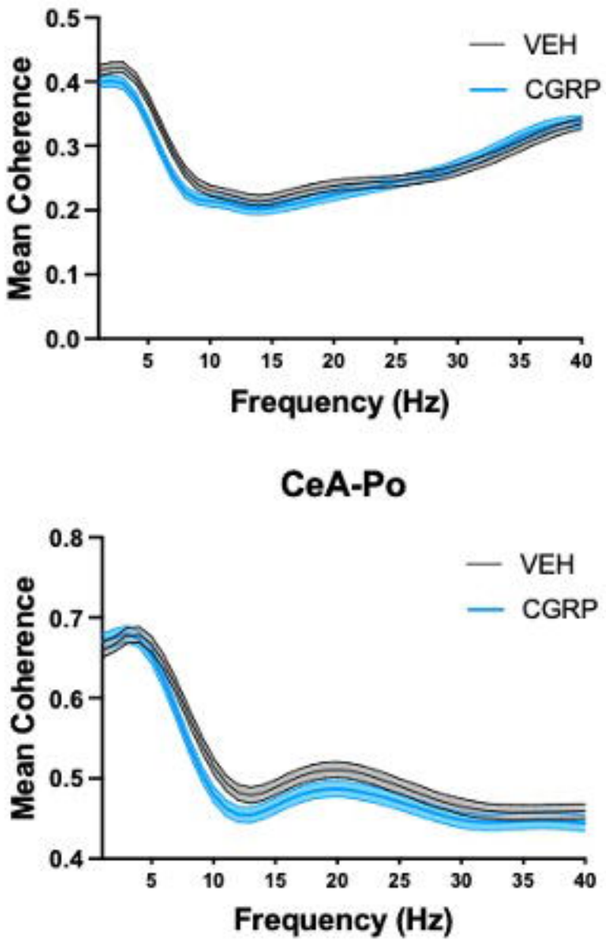

B.

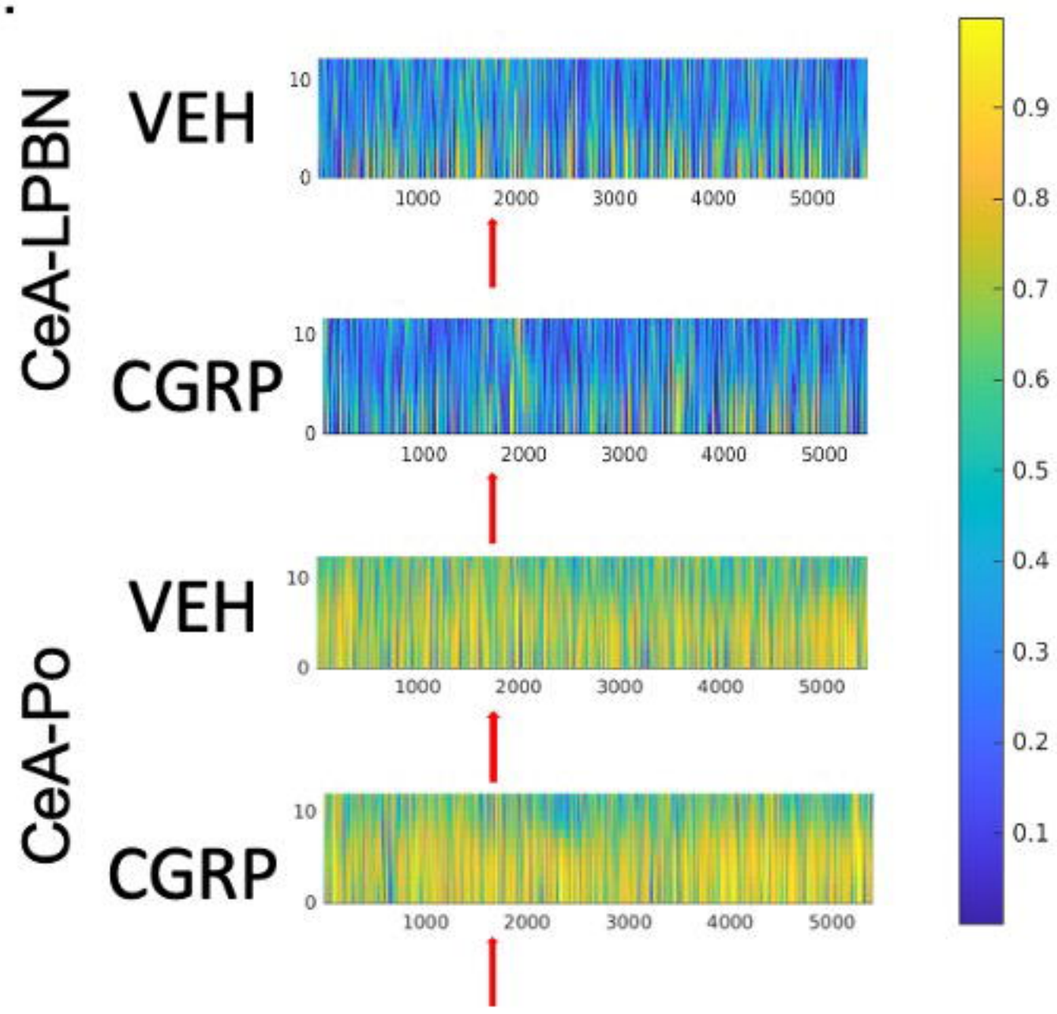

C.

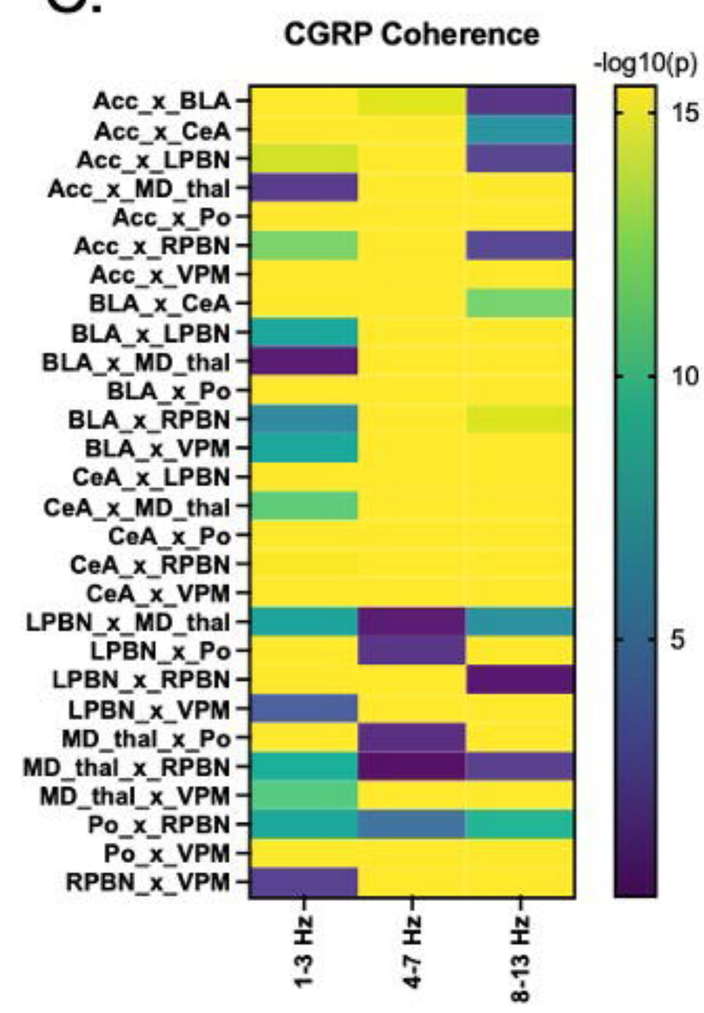

D. CeA-LPBN (4-7 Hz)

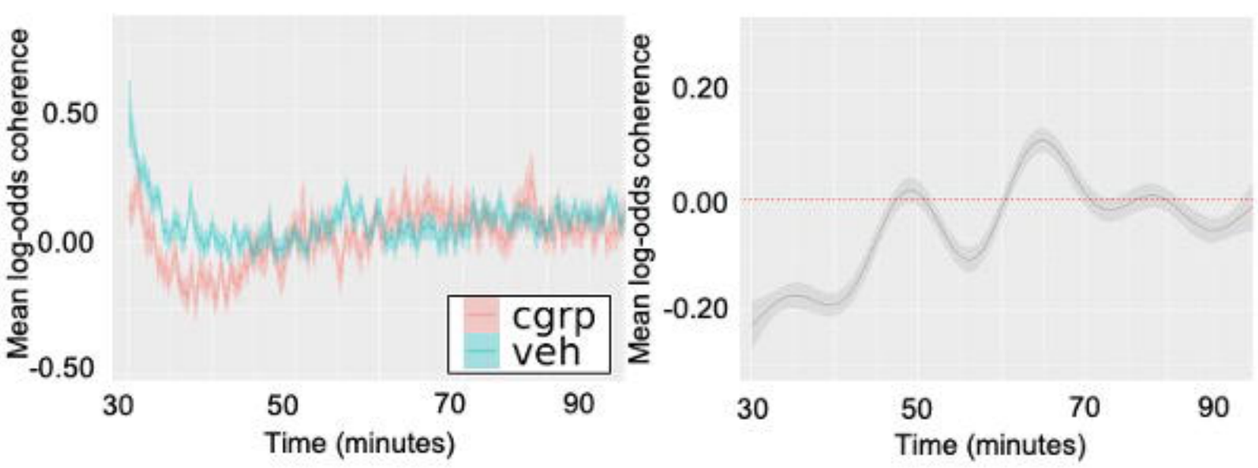

E. CeA-Po (8-13 Hz)

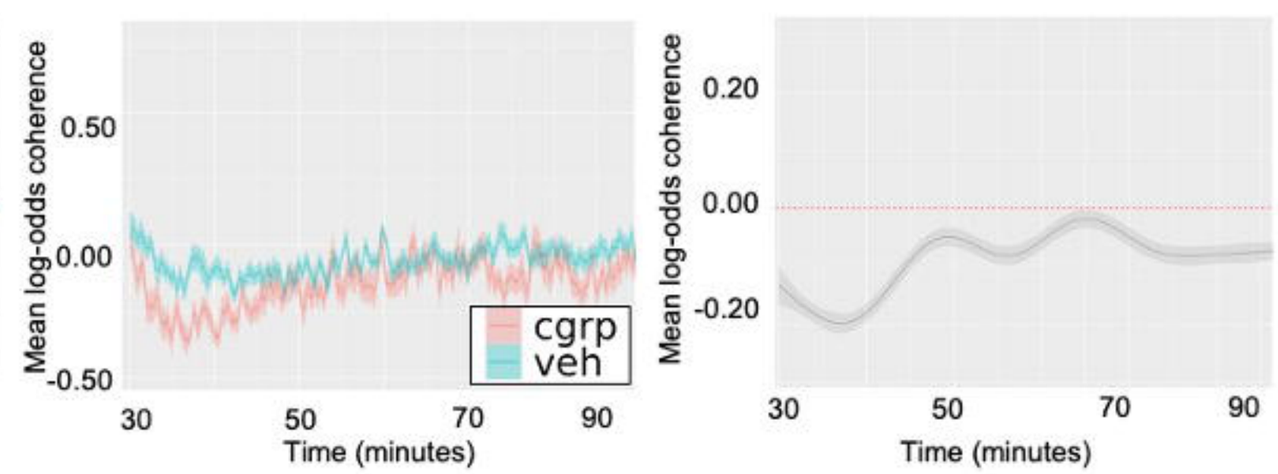

F. BLA-VPM (8-13 Hz)

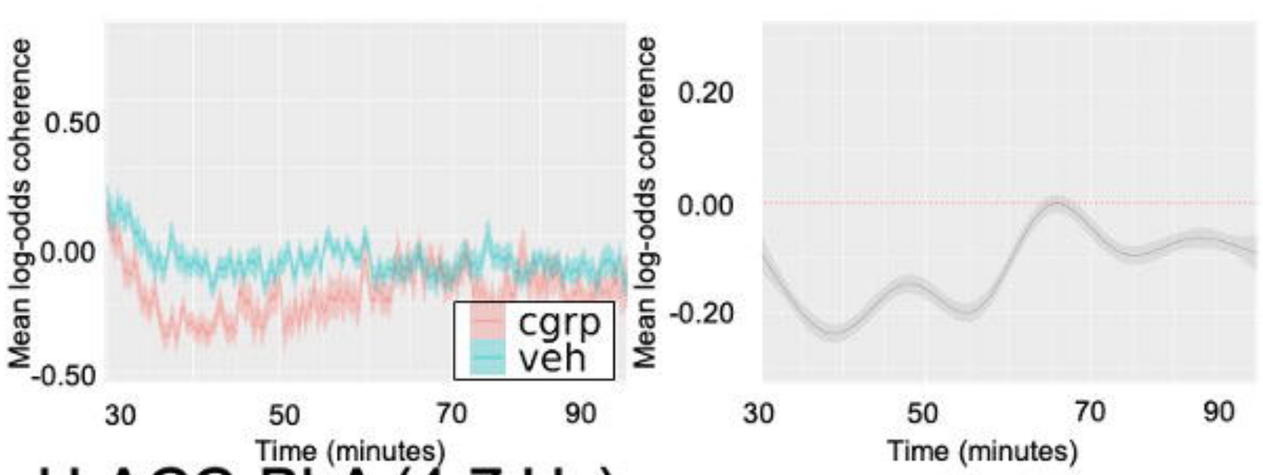

G. LPBN-Po (8-13 Hz)

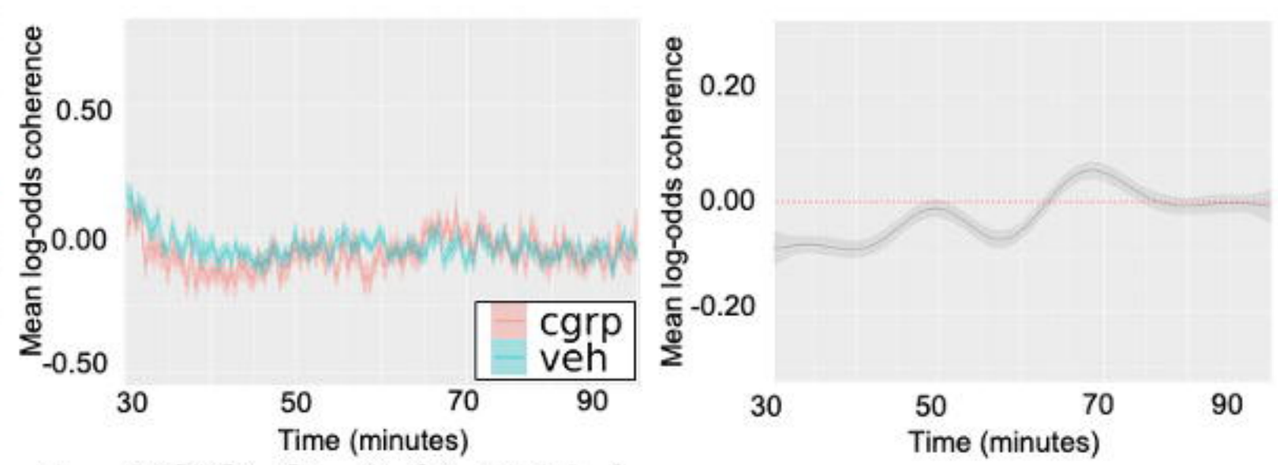

H. ACC-BLA (4-7 Hz)

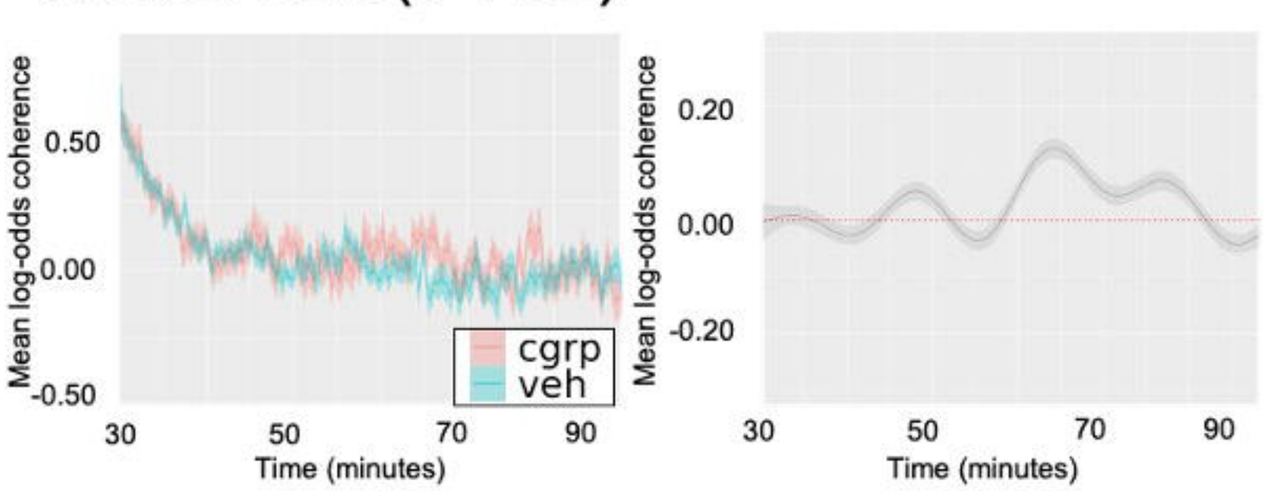

I. ACC-CeA (4-7 Hz)

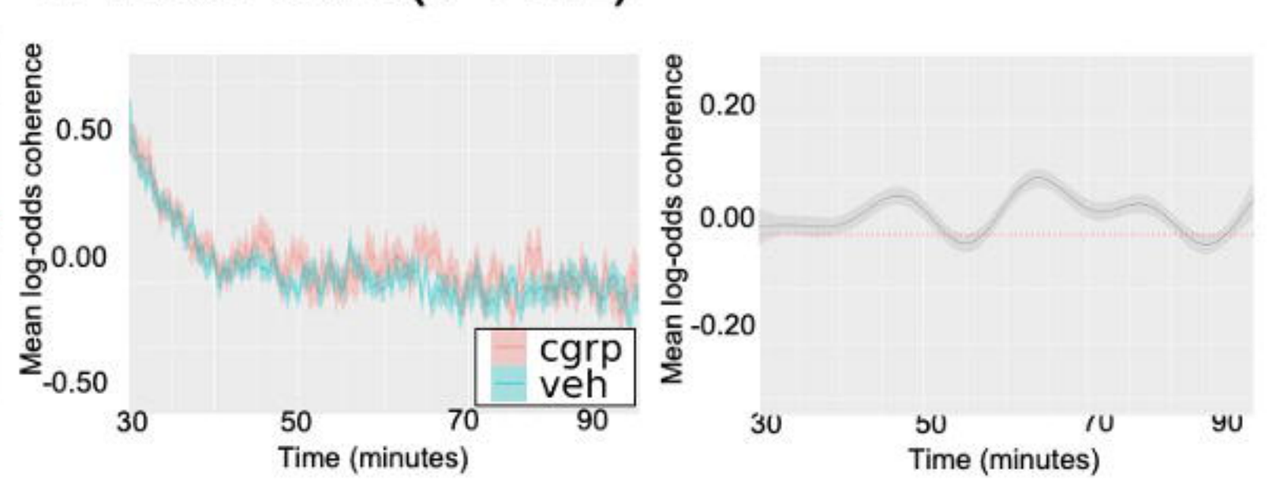

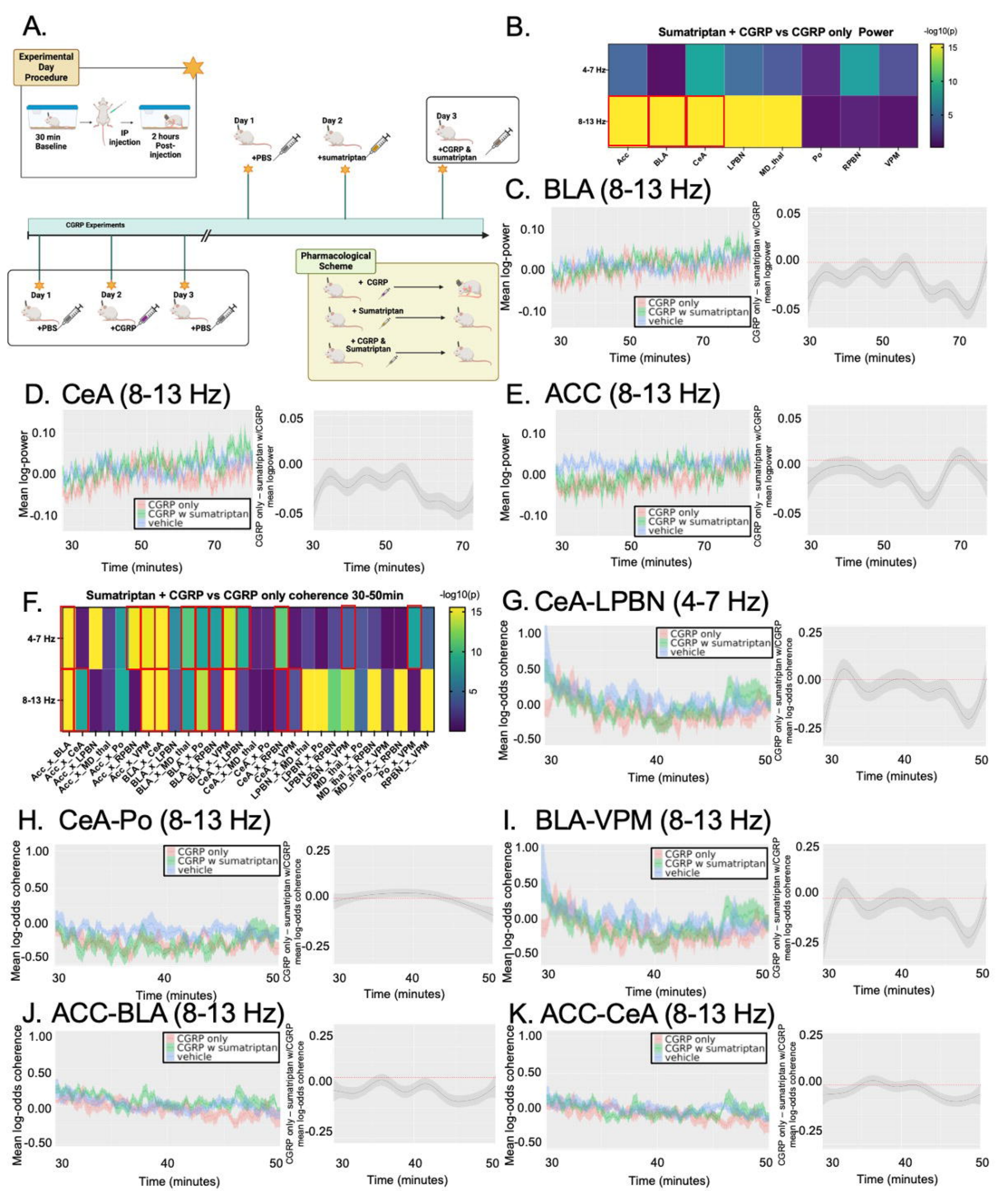
A.
Experimental Day Procedure
30 min Baseline
IP injection
2 hours Post-injection
Day 1
+PBS
Day 2
+sumatriptan
Day 3
+CGRP & sumatriptan
CGRP Experiments
Day 1
+PBS
Day 2
+CGRP
Day 3
+PBS
Pharmacological Scheme
+ CGRP
+ Sumatriptan
+ CGRP & Sumatriptan
B.
Sumatriptan + CGRP vs CGRP only Power
-log10(p)
4-7 Hz
8-13 Hz
Acc
BLA
CeA
LPBN
MD_thal
Po
RPBN
VPM
C. BLA (8-13 Hz)
D. CeA (8-13 Hz)
E. ACC (8-13 Hz)
F.
Sumatriptan + CGRP vs CGRP only coherence 30-50min
G. CeA-LPBN (4-7 Hz)
H. CeA-Po (8-13 Hz)
I. BLA-VPM (8-13 Hz)
J. ACC-BLA (8-13 Hz)
K. ACC-CeA (8-13 Hz)
Mean log-power
Mean log-odds coherence
CGRP only – sumatriptan w/CGRP mean logpower
CGRP only – sumatriptan w/CGRP mean log-odds coherence
CGRP only
CGRP w sumatriptan
vehicle
Time (minutes)

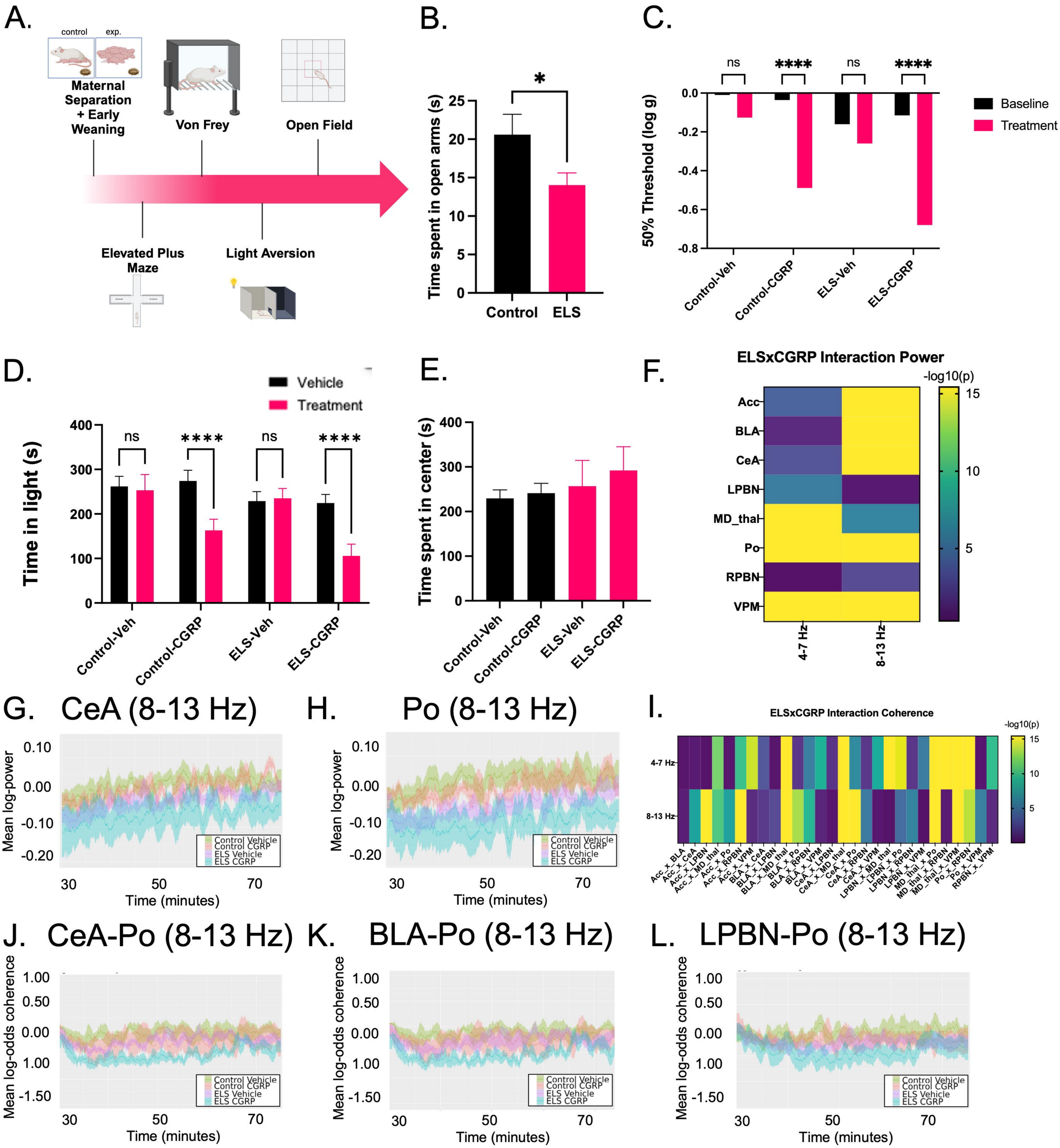
A.
control
exp.
Maternal Separation + Early Weaning
Von Frey
Open Field
Elevated Plus Maze
Light Aversion
B.
Time spent in open arms (s)
Control
ELS
C.
50% Threshold (log g)
ns
****
ns
****
Baseline
Treatment
Control-Veh
Control-CGRP
ELS-Veh
ELS-CGRP
D.
Vehicle
Treatment
Time in light (s)
E.
Time spent in center (s)
F.
ELSxCGRP Interaction Power
-log10(p)
Acc
BLA
CeA
LPBN
MD_thal
Po
RPBN
VPM
4-7 Hz
8-13 Hz
G. CeA (8-13 Hz)
H. Po (8-13 Hz)
I.
ELSxCGRP Interaction Coherence
Mean log-power
Control Vehicle
Control CGRP
ELS Vehicle
ELS CGRP
Time (minutes)
J. CeA-Po (8-13 Hz)
K. BLA-Po (8-13 Hz)
L. LPBN-Po (8-13 Hz)
Mean log-odds coherence

A.

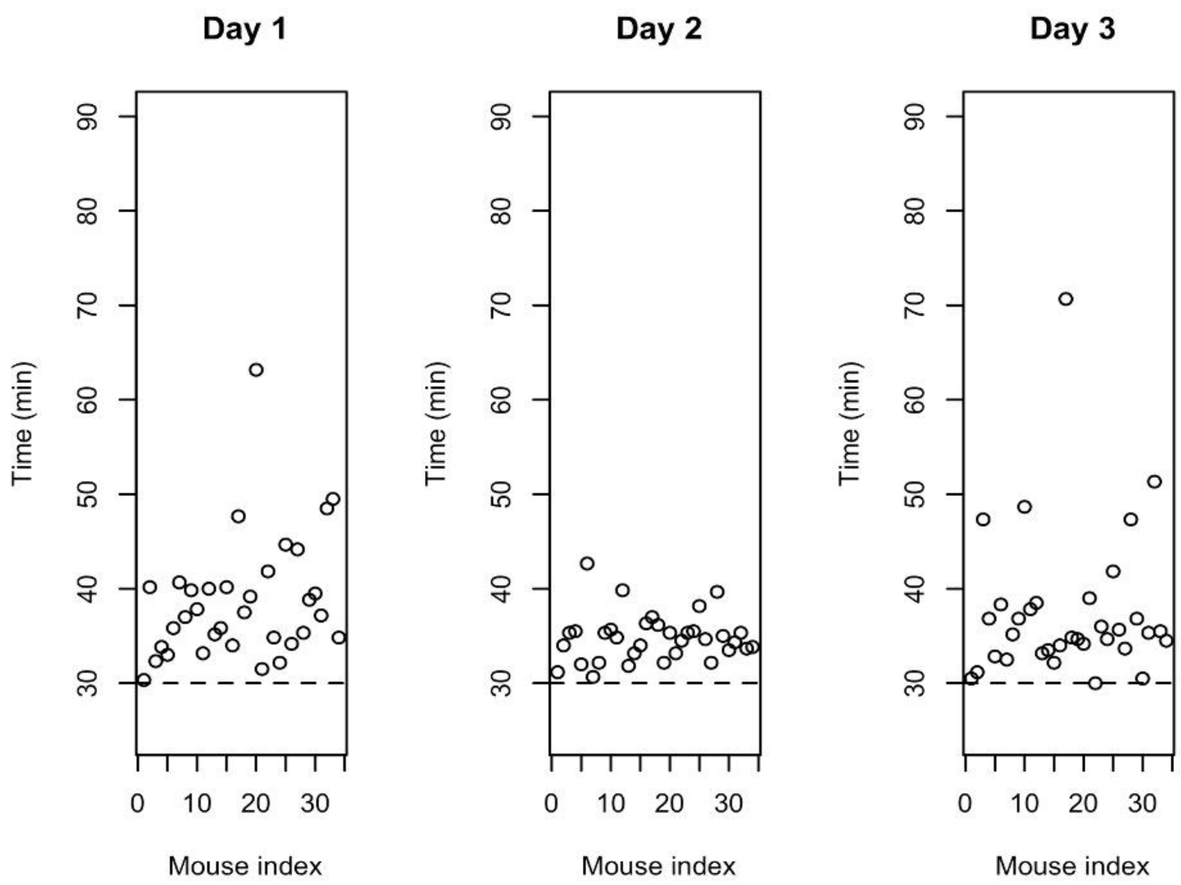

B.

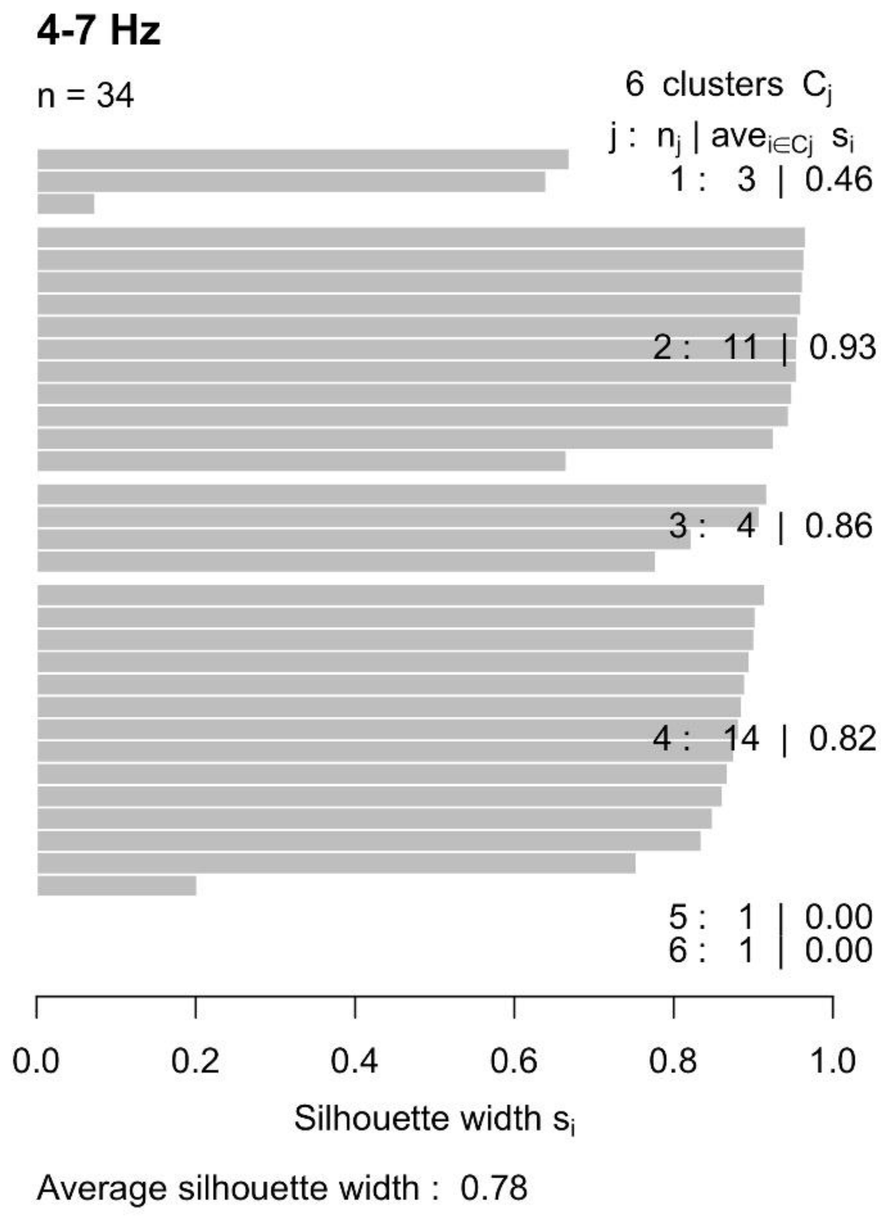

C.

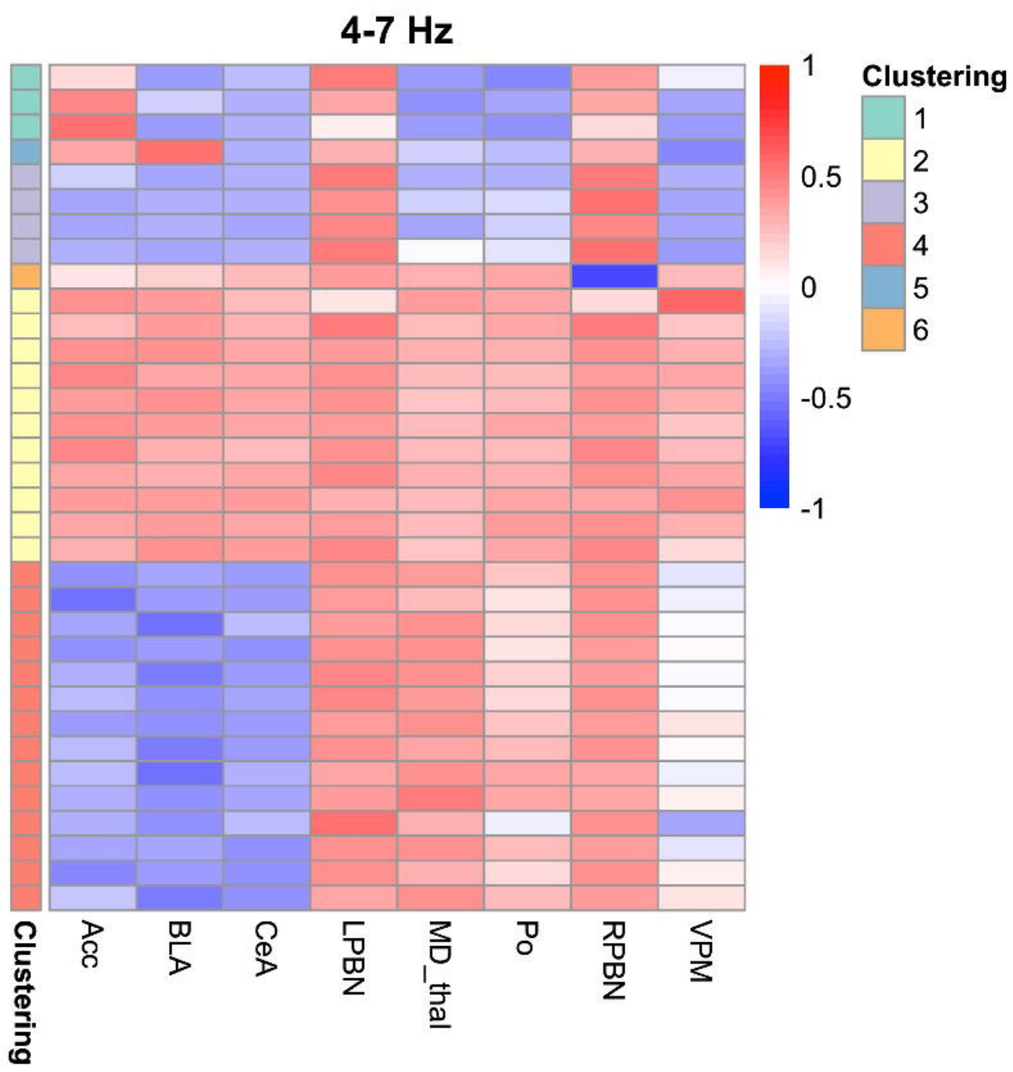

D.

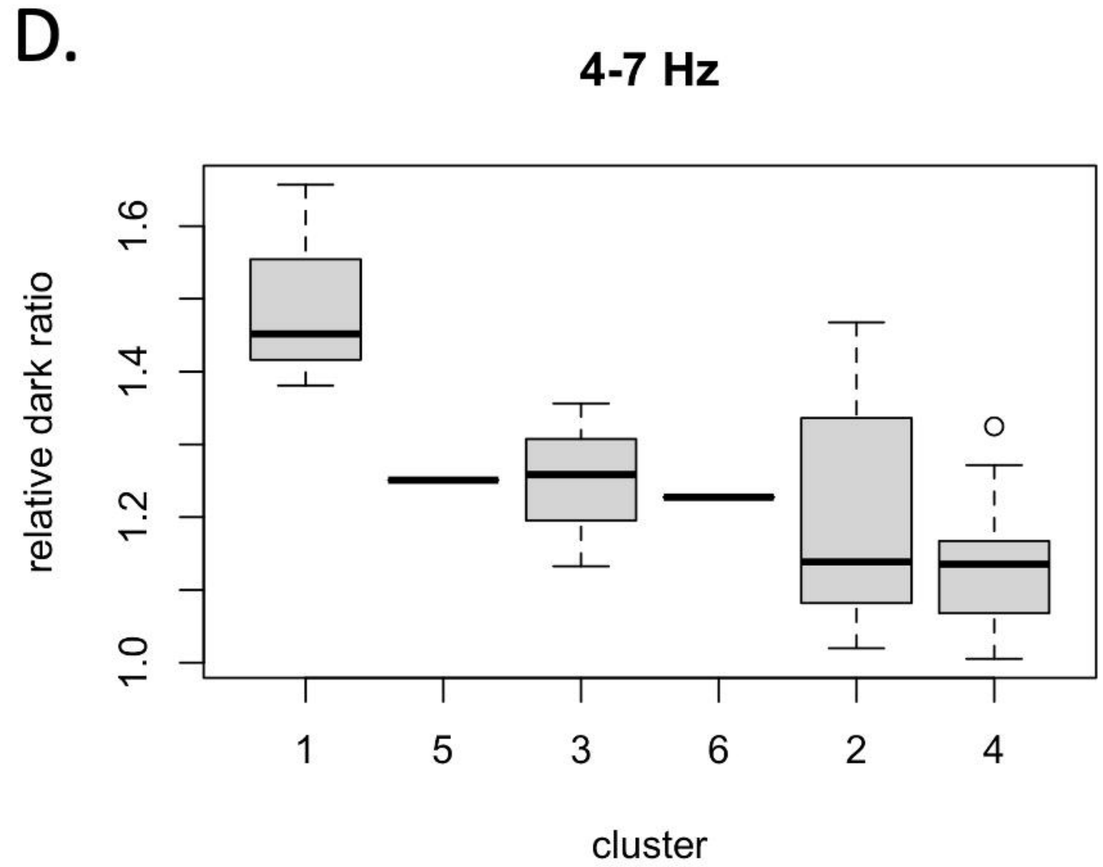

E.

4-7 Hz cluster 1

	LPBN	RPBN	Acc	MD_thal	Po	VPM	BLA	CeA
LPBN	0.00	0.01	0.05	0.07	0.07	0.06	0.04	0.05
RPBN	0.01	0.00	0.04	0.07	0.06	0.06	0.04	0.05
Acc	0.05	0.04	0.00	0.06	0.06	0.02	0.06	0.04
MD_thal	0.07	0.07	0.06	0.00	0.00	0.01	-0.01	0.00
Po	0.07	0.06	0.06	0.00	0.00	0.03	-0.01	0.01
VPM	0.06	0.06	0.02	0.01	0.03	0.00	-0.03	-0.03
BLA	0.04	0.04	0.06	-0.01	-0.01	-0.03	0.00	0.00
CeA	0.05	0.05	0.04	0.00	0.01	-0.03	0.00	0.00

4-7 Hz cluster 2

	LPBN	RPBN	MD_thal	Po	VPM	Acc	BLA	CeA
LPBN	0.00	0.00	-0.07	-0.10	-0.14	-0.21	-0.20	-0.19
RPBN	0.00	0.00	-0.08	-0.10	-0.14	-0.20	-0.19	-0.18
MD_thal	-0.07	-0.08	0.00	-0.03	-0.03	-0.11	-0.11	-0.09
Po	-0.10	-0.10	-0.03	0.00	-0.04	-0.10	-0.11	-0.09
VPM	-0.14	-0.14	-0.03	-0.04	0.00	-0.07	-0.10	-0.08
Acc	-0.21	-0.20	-0.11	-0.10	-0.07	0.00	-0.04	-0.03
BLA	-0.20	-0.19	-0.11	-0.11	-0.10	-0.04	0.00	-0.01
CeA	-0.19	-0.18	-0.09	-0.09	-0.08	-0.03	-0.01	0.00

4-7 Hz cluster 3

	LPBN	RPBN	MD_thal	Po	VPM	Acc	BLA	CeA
LPBN	0.00	0.02	-0.10	-0.07	-0.15	-0.17	-0.15	-0.14
RPBN	0.02	0.00	-0.11	-0.08	-0.16	-0.17	-0.15	-0.14
MD_thal	-0.10	-0.11	0.00	0.01	-0.02	-0.05	-0.06	-0.05
Po	-0.07	-0.08	0.01	0.00	-0.02	-0.01	-0.02	-0.03
VPM	-0.15	-0.16	-0.02	-0.02	0.00	-0.01	-0.01	0.00
Acc	-0.17	-0.17	-0.05	-0.01	-0.01	0.00	-0.03	-0.02
BLA	-0.15	-0.15	-0.06	-0.02	-0.01	-0.03	0.00	0.00
CeA	-0.14	-0.14	-0.05	-0.03	0.00	-0.02	0.00	0.00

4-7 Hz cluster 4

	LPBN	RPBN	MD_thal	Po	VPM	Acc	BLA	CeA
LPBN	0.00	0.01	0.01	-0.02	-0.05	-0.10	-0.11	-0.10
RPBN	0.01	0.00	0.01	-0.01	-0.05	-0.10	-0.10	-0.09
MD_thal	0.01	0.01	0.00	-0.01	-0.02	-0.08	-0.10	-0.08
Po	-0.02	-0.01	-0.01	0.00	-0.02	-0.05	-0.07	-0.06
VPM	-0.05	-0.05	-0.02	-0.02	0.00	-0.03	-0.05	-0.04
Acc	-0.10	-0.10	-0.08	-0.05	-0.03	0.00	-0.01	-0.01
BLA	-0.11	-0.10	-0.10	-0.07	-0.05	-0.01	0.00	-0.01
CeA	-0.10	-0.09	-0.08	-0.06	-0.04	-0.01	-0.01	0.00

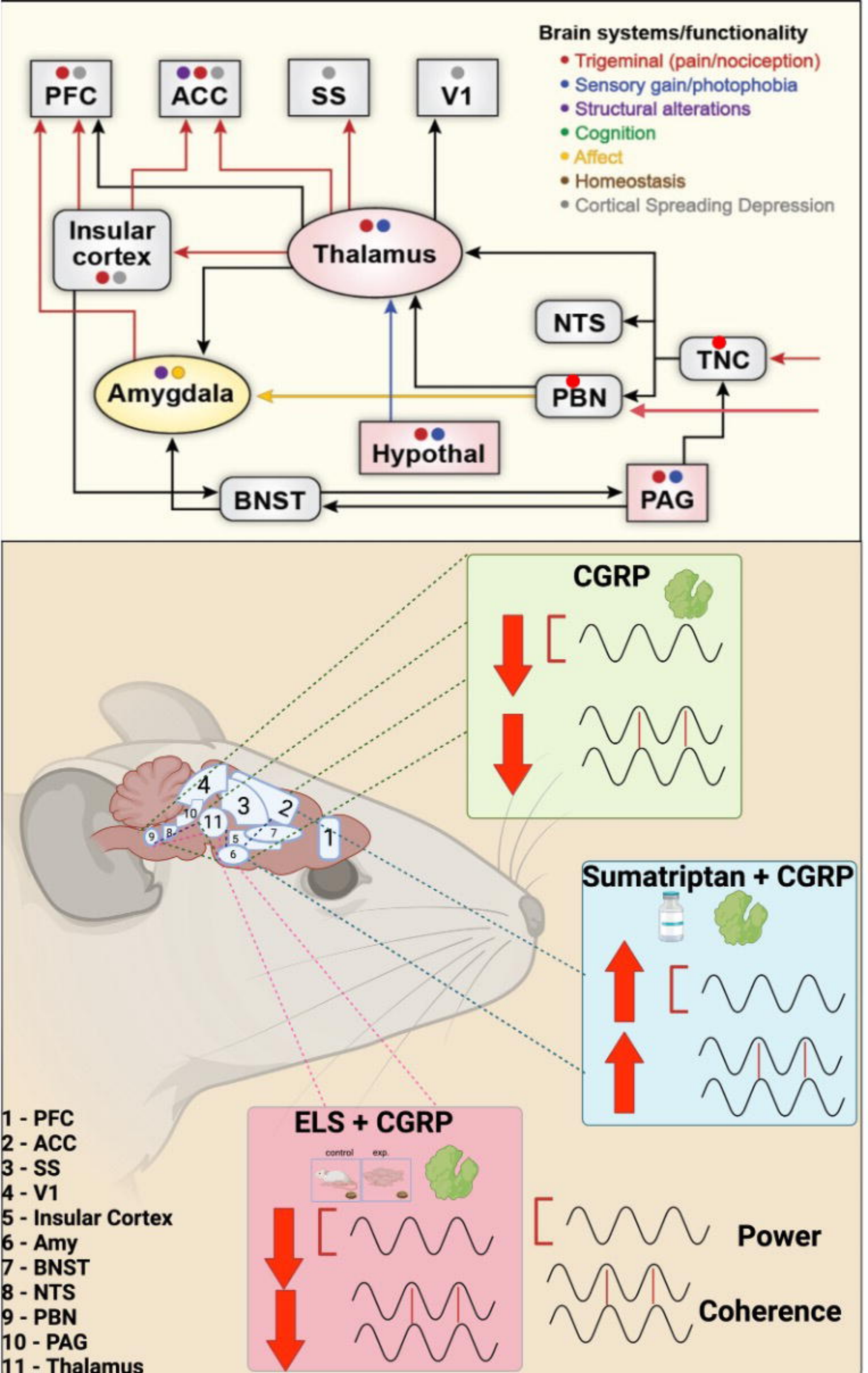
Brain systems/functionality
Trigeminal (pain/nociception)
Sensory gain/photophobia
Structural alterations
Cognition
Affect
Homeostasis
Cortical Spreading Depression
PFC
ACC
SS
V1
Insular cortex
Thalamus
NTS
TNC
Amygdala
PBN
Hypothal
BNST
PAG
CGRP
Sumatriptan + CGRP
ELS + CGRP
control
exp.
Power
Coherence
1 - PFC
2 - ACC
3 - SS
4 - V1
5 - Insular Cortex
6 - Amy
7 - BNST
8 - NTS
9 - PBN
10 - PAG
11 - Thalamus